Numerical Analysis of Flame Shape Impact on the Performance of Fuel Staging in a Lean-Burn Aeronautical Burner

Leo Cunha Caldeira Mesquita, Aymeric Vié, Sébastien Ducruix

NUMERICAL ANALYSIS OF FLAME SHAPE IMPACT ON THE PERFORMANCE OF FUEL STAGING IN A LEAN-BURN AERONAUTICAL BURNER

Léo C. C. Mesquita[1,*], Aymeric Vié[1], Sébastien Ducruix[1]

[1]Université Paris-Saclay, CNRS, CentraleSupélec, Laboratoire EM2C, 91190, Gif-sur-Yvette, France

ABSTRACT

The BIMER combustor is a lab-scale burner investigating fuel staging techniques as a stabilisation strategy for lean premixed prevaporized combustion for aeronautical applications. Two stages compose its injection system: the pilot and the multipoint stages. The staging factor is defined as the ratio of fuel mass flowrate injected through the pilot stage over the total one. As three flames shapes were found experimentally, Large-Eddy Simulations are performed in this study to assess the impact of the flame shape in the combustion regime and stability of the burner. Two operating conditions were explored experimentally (pilot-only and multipoint-dominated) to validate the simulations and compare the three flames. An additional multipoint-only condition is also investigated for the V flame. The burning regimes were compared (premixed and non-premixed) and noise signatures as a function of fuel staging, to check whether these flames could benefit from the staging strategy. The M and Tulip flame combustion regimes are little affected by fuel staging, remaining mostly premixed and non-premixed, respectively, regardless of fuel staging. In opposition, the V flame changes from being mostly non-premixed to completely premixed, when the injection is changed from pilot-only to multipoint-only. For the same staging evolution, the V flame also emits less noise for the investigated points. The V flame shape is probably the only one that allows this burner to benefit from an efficient fuel staging operating strategy.

Keywords: LPP combustion, staged burners, partially premixed, multipoint injection, flame shape

NOMENCLATURE

BIMER	*Banc à Injection Multiple pour les Ecoulements Réactifs*
BVB	Bubble Vortex Breakdown
CVB	Conic Vortex Breakdown
CRZ	Central Recirculation Zone
ISL	Inner Shear Layer
FI	Flame Index
HVC	Helical Vortex Core
LES	Large-Eddy Simulations
LPP	Lean Premixed Prevaporized
ORZ	Outer Recirculation Zone
OSL	Outer Shear Layer
PVC	Precessing Vortex Core
SMD	Sauter Mean Diameter
SPL	Sound Pressure Level
α	Staging factor
ϕ	Equivalence ratio

*Corresponding author: leo.mesquita@rolls-royce.com , currently at Rolls-Royce plc., Hot End Centre of Excellence, Derby, UK

1. INTRODUCTION

Lean Premixed Prevaporized (LPP) combustors often show unstable behaviours (flashback, thermo-acoustic instabilities, flame blow-off) due to their intrinsic tendency to present strong flow and flame dynamics [1, 2]. Staged multipoint injection is being investigated as a technical solution to control these unwanted phenomena in gas turbines, and aircraft swirled burners. The BIMER combustor, studied in this paper, was designed based on a Safran Aircraft Engines prototype at the EM2C Laboratory and has been operated for several years with the objective of better understanding the complex processes involved in the operation of aeronautical staged multipoint swirled burners. The BIMER burner is composed of two stages: the pilot stage, where a pressure-swirl nozzle sustains a spray flame and stabilises the system, and the multipoint stage, where a multipoint fuel injector achieves premixed combustion. Fuel can be distributed between them to change the flame structure and adapt it according to the operation requirements. It is crucial then to understand how the injection regime and fuel distribution impact the burner response.

Three flame shapes were observed during the experimental investigation of this burner: M, Tulip and V, each showing different characteristics. The M flame is a lifted flame, aerodynamically stabilised inside the chamber by the Bubble Vortex Breakdown (BVB) mode [3–5]. The Tulip flame presents similar aerodynamics and stabilisation mechanism as the M flame, with an additional burning branch attached to the pilot spray near the injection system. The V flame, however, modifies the flow aerodynamics to stabilise a Conical Vortex Breakdown (CVB) [6, 7], which results in a larger central recirculation zone, causing a different flame shape and a different dynamical behaviour.

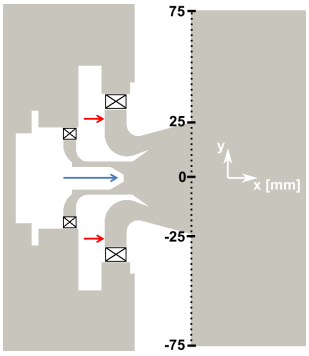

FIGURE 1: 2D CUT OF THE INJECTOR: PILOT INJECTOR LOCATION (BLUE ARROW) AND RADIAL POSITION OF MULTI-POINT INJECTION HOLES (RED ARROWS). FLOW FROM LEFT TO RIGHT.

Consequently, the V flame is stabilised over the Inner Shear Layer (ISL), and burns attached to the pilot spray. Therefore, this multi-stable behaviour opens the question of which of the flame shapes is more suitable for this staged burner. This paper objective is then to evaluate the performances of these three flames in the context of an aeronautical liquid-fuelled staged burner. Various flame shapes and their interactions with injection regimes were studied in the past, mainly for gaseous fuels in staged [8, 9] or non-staged burners [10, 11]. With liquid fuels, the focus was on flame transition mechanisms [12–17] or on comparing the flame shapes for different conditions [18], and not on the performance of the different flame shapes when fuel staging was applied.

Therefore, this work presents an original and detailed comparison of the fuel staging impact on different flame shapes in a liquid-fuelled aeronautical lean burner. We compare the flames in terms of performance and their suitability for staged operation based on how they respond to the change in staging. To do so, we perform Large-Eddy Simulations of each flame in two staging conditions where experimental data was available, and the validation of the simulations was possible [19]: full pilot and multipoint-dominated LPP operations. We then analyse the flame structures in each condition and compare them. The ideal flame should respond to the change in injection regime, going from a more stable, non-premixed flame in pilot-only conditions to a premixed flame in multipoint-dominated operation. Therefore, in this work, the flame performance is evaluated using the potential control of its structure and dynamics by the injection system.

The paper is organised as follows: first, we describe the burner, followed by the numerical setup. Then we present the simulation results for each flame, analysing and discussing their properties. Finally, we conclude by presenting which of the three flames is ideal for the present staged burner operation.

2. THE BIMER COMBUSTOR

The BIMER is a lab-scale aeronautical combustor composed of a cylindrical plenum (containing the two-staged swirled burner) and a rectangular combustion chamber (squared cross-section $150 \times 150\,\text{mm}^2$ and 500 mm long). The two lateral sides of the combustion chamber are silica windows to provide visual access. The entrance, top and bottom walls are made of stainless steel and water-cooled for thermal regulation. Its staged burner (Fig. 1) is composed of two co-swirling stages, each containing a different injection system. The pilot stage swirler has a geometric swirl number of 0.6 and 15 % of the air mass flow rate passes through this stage. The pilot injector is a pressure-swirl nozzle, which produces a hollow cone spray with a 30° half-spray angle. The multipoint stage swirler has a geometric swirl number of 1 and 85 % of the air mass flow rate passes through this stage. The fuel is injected through 10 holes (0.3 mm diameter, equally spaced at swirler vanes' exits) in a jet-in-crossflow configuration.

3. FLOW MODELLING AND NUMERICAL SET-UP

We use the AVBP code, co-developed by CERFACS and IFPEN [20], to perform the 3D reacting LES of the compressible multi-species Navier-Stokes equations of the BIMER combustor. The sub-grid scales are modelled by the WALE model [21]. We use a Two-step Taylor Galerkin (TTGC) finite elements scheme (3rd order in space and in time) with artificial diffusion [22]. The Navier-Stokes Characteristic Boundary Conditions (NSCBC) [23] model the gaseous inlet and outlet boundary conditions. We model the wall-gas interaction as no-slip. To model the water-cooling of the chamber walls, we apply an isothermal condition to the entrance, bottom and top walls, using temperature values measured experimentally. All the other walls and surfaces in the domain are considered adiabatic.

To model turbulent combustion, we use the Thickened Flame model (TFLES) [24] coupled with the Charlette's efficiency function [25]. In the BIMER combustor, part of the flame may burn in a non-premixed regime, as the spray not always prevaporizes and premixes entirely. As TFLES is for premixed flames, it introduces an error in these non-premixed regions. This error is however believed to be marginal regarding the different validations of the LES of the BIMER combustor with TFLES even with non-premixed regions [16–19, 26]. We use the BFER reduced chemical mechanism for kerosene [27] and unity Lewis numbers are assumed, an acceptable simplification considering the very simple combustion and chemistry models.

We use a 32 million tetrahedra mesh for the simulations, which results from a convergence study[28], and from several validations against experimental data performed in [19]. This mesh results in a flame thickening factor between 5 and 7 in the flame zone, which is reasonable to properly track flame dynamics. The liquid phase is represented by a Lagrangian point-particle modelling [29]. The Abramzon-Sirignano model [30] is used fo droplet vaporization. As some fuel film formation was observed over the burner divergent during the experiments [31], the droplet-wall interaction is modelled as a slip condition, to mimic in a very simplistic way a film-like behaviour. We model the pilot spray as a hollow cone with a spray half angle of 30° [31] with a calibrated version of the FIMUR model [26]. For the multipoint injection, droplets are injected at the position of the multipoint holes with a normal velocity. The diameter distributions for all injectors were obtained from experiments [31], see appendix A for validation.

The three flames archetypes studied in this work were initialised by mimicking the experimental ignition procedure [16]. First, in a full pilot injection condition, the non-reacting flow with spray is simulated. Then, a flame kernel is initialised and develops into a flame. Depending on the operating conditions

TABLE 1: OPERATING POINTS FOR THE V FLAME

Point name	OP_1	OP_2	$OP_{2,\alpha=0\%}$
$\dot{m}_{air}$	$32.3g/s$	$43.1g/s$	$43.1g/s$
T_{air}	$473K$	$433K$	$433K$
$\dot{m}_{fuel}$	$1.02g/s$	$1.64g/s$	$1.64g/s$
$Power$	$45.9kW$	$73.9kW$	$73.9kW$
α	100%	15%	0%
ϕ, ϕ_{pilot}, ϕ_{multi}	0.47, 3.64, -	0.57, 0.66, 0.56	0.57, -, 0.65

and location of the kernel, a V, Tulip or M flame shape can be obtained. Once these flames are stabilised, the operating conditions are changed to, first, the pilot-only conditions studied in this work (OP_1), and, then, to the LPP-representative conditions (OP_2).

In the following we define the Flame Index (FI) as the product of positive Heat Release Rate and the Takeno index $FI = max(HRR, 0) \cdot \nabla Y_{Kero} \cdot \nabla Y_{O_2} / \left|\nabla Y_{Kero} \cdot \nabla Y_{O_2}\right|$. Furthermore, all time-averaged statistics are gathered over 40 ms.

4. RESULTS

4.1 V flames

We first investigate the V flame shape, stable for the largest range of staging factors in [31], from pilot-only ($\alpha = 100\%$) to multipoint-only ($\alpha = 0\%$) operation. We focus our analysis on three conditions, OP_1, OP_2 and $OP_{2,\alpha=0\%}$ (see Tab. 1), to assess the response of this flame to the injection regime variation. These results allow the analysis of the V flame with the two extreme values (i.e. $\alpha = 100\%$ and $\alpha = 0\%$) and an intermediate case representative of a practical LPP operation ($\alpha = 15\%$).

The V flame is so called because of its constantly diverging shape from its roots, similar to the letter "V". This can be seen in Fig. 2, where instantaneous snapshots of the V flame are shown for the three operating conditions OP_1, OP_2 and $OP_{2,\alpha=0\%}$. The similarities between the three flames point out major characteristics, and the flame can be divided into three parts: the root of the flame is the part inside the divergent section of the burner attached to the spray; the branches of the flame are the most representative part, penetrating the combustion chamber and responsible for most of the heat released; and the trunk is the transverse part burning inside the CRZ and connected at the intersection between the flame roots and the flame branches. This nomenclature is used to describe the two attached shapes (V and Tulip).

4.1.1 OP1. First observing the OP_1 V flame, the Flame index (Fig. 2a center) shows the flame attached to the pilot spray and stabilised around the conic CRZ (characteristic of the CVB mode) and divides it into premixed and non-premixed combustion regimes. Despite the lean global equivalence ratio, this pilot-only condition corresponds to a theoretical pilot stage local equivalence ratio at $\phi_{pilot} = 3.64$. The strong spray creates a fuel-rich zone inside the divergent, where gaseous and liquid fuel concentrate. The flame roots are anchored at the spray in this region, burning mostly in a non-premixed regime, with a core region of premixed combustion. Indeed, the flame root represents the highest local heat release rate zone, both in premixed and non-premixed regimes. The long flame branches reach the walls, and burn in a premixed regime at the lean global equivalence ratio ($\phi = 0.5$). The injected droplet distribution contains a significant amount of large droplets, which penetrate inside the combustion chamber and interact with all of the lengths of the flame branches. The large droplets that are injected with angles similar to the diverging swirling jet one (between 30 and 45) mainly reach the walls, some of them being thrown inside the CRZ by the flow. The flame trunk, located between the spray/fuel-rich zone and the burnt gases, burns mostly in a non-premixed regime. Thus, despite the whole system being designed to promote lean premixed combustion, using only the pilot injector implies a considerable portion of non-premixed rich combustion, as the flame is attached to and strongly interacts with the pilot spray.

The distribution of FI against mixture fraction (Fig. 2a right) sheds further light on how combustion takes place with respect to the combustion regime. Being coloured by the percentage of flame volume, it points out that while the majority of the flame is around the global equivalence ratio ($z_{global} = 0.0323$), this zone corresponds only to 53% of the total heat released, as shown by the cumulative sum of power over the mixture fraction. Indeed, crossing the information with average fields, it is possible to see that the flame branches (low heat release rate at global mixture fraction value) correspond to most of the flame volume, and to the combustion peak around the global equivalence ratio. The rest of the heat release, which spreads over the stoichiometric and fuel-rich zones, is then concentrated on the flame root and trunk, portions attached to the pilot spray. This shows how these two much smaller zones of the flame, confined inside the divergent, are responsible for closely half of the total power. This highlights the role that fuel staging and mixing should play in reducing non-premixed combustion, as almost all of it is concentrated in the flame root and trunk. Indeed, even if the global equivalence ratio is lean, the *theoretical* stage equivalence ratio, calculated using fuel and air coming a single stage, is very high, $\phi_{pilot} = 3.64$. This illustrates how combustion close to the pilot stage is rich and likely non-premixed. This is confirmed by the fact that the flame root and trunk (stabilised around the pilot spray) are responsible for 47% of the total heat released, all of which occurs over the global equivalence ratio, with 26% of the total (11.7 kW/44.5 kW) on fuel-rich conditions. For the total heat release, the power splits in approximately 84% for the premixed regime (37.4 kW) and 16% for the non-premixed one (7.1 kW).

The time-averaged field of the percentage of *pilot air* (Fig. 3a) gives more insight into the flame structure and how each part of the flame is fed by the air. The pilot air is dominant (over 50% - red and orange regions) just downstream of its entry inside the divergent, with the PVC attracting the pilot air inside the CRZ and trapping it there. Thus, the flame roots, that burn in stoichiometric and rich conditions, are fed almost exclusively by pilot stage air, which only represents 13% of the total air mass flow rate. This shows that the information given by the theoretical stage equivalence ratio ($\phi_{pilot} = 3.64$) is representative of the local burning conditions. Thus, this low availability of air results in poor mixing in this zone, high local heat release rate and non-premixed burning. In opposition, the flame trunk, the other portion of the flame burning mostly in a non-premixed regime, is inside the CRZ and fed mainly by recirculated gases at the staging ratio. Thus, the high staging factor seems to be more

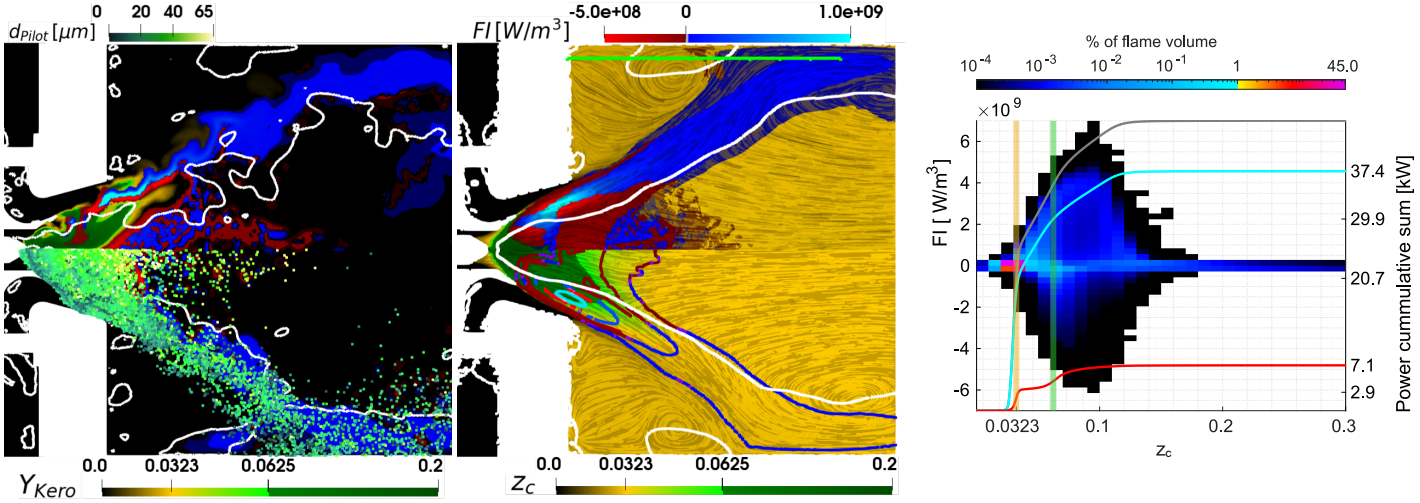

(a) OP_1

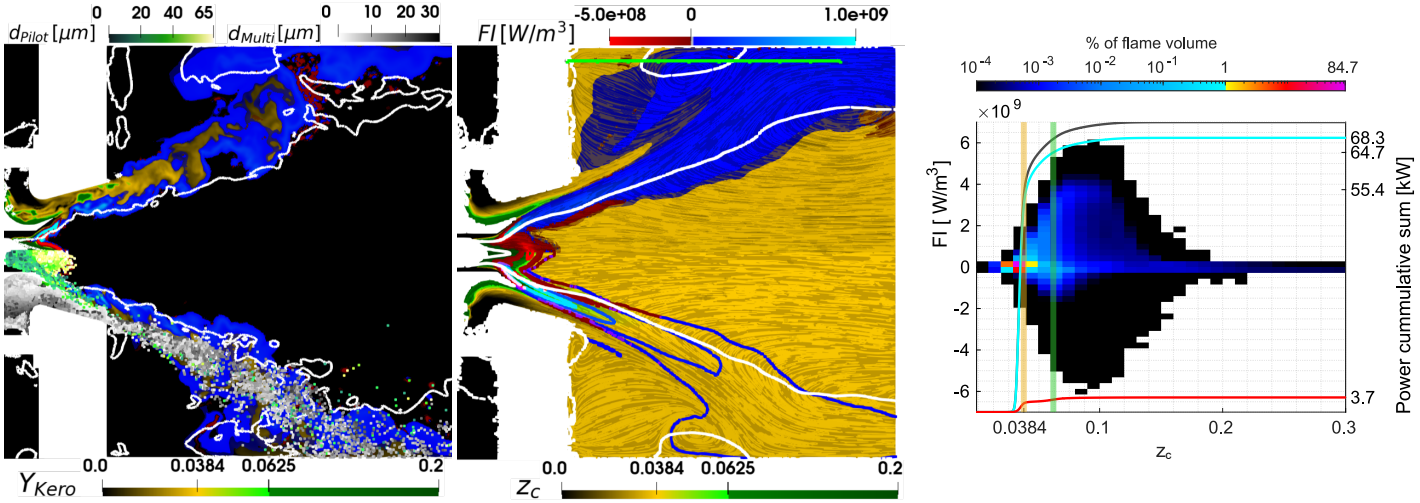

(b) OP_2

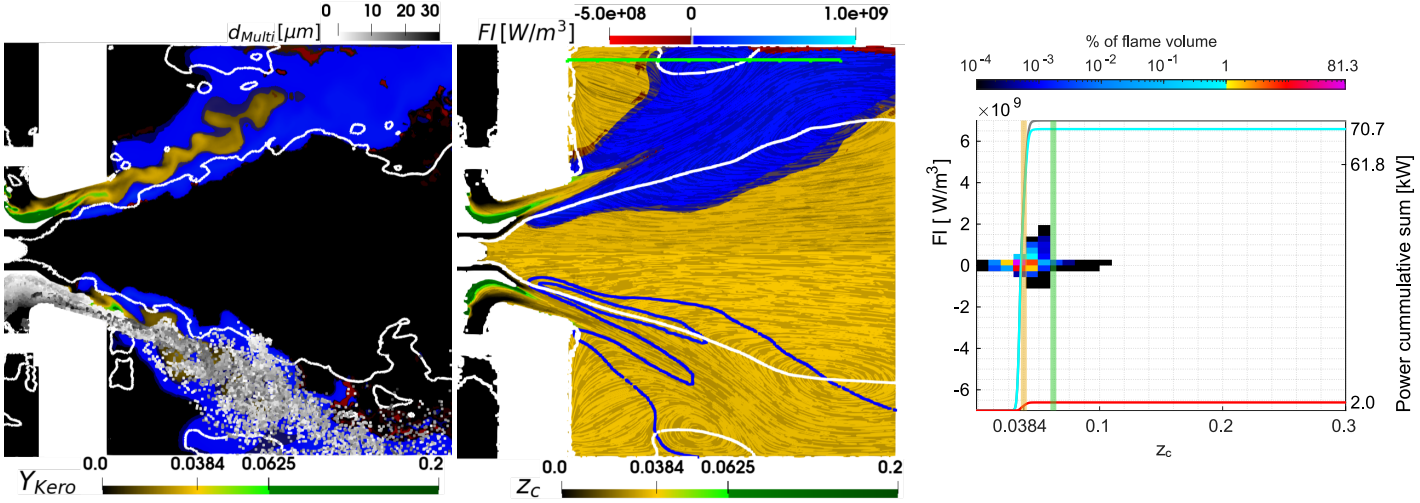

(c) $OP_{2,\alpha=0\%}$

FIGURE 2: V FLAMES. LEFT COLUMN: Y_{KERO} INSTANTANEOUS FIELDS WITH FI SUPERIMPOSED AND ISO-CONTOURS OF ZERO AXIAL VELOCITY (WHITE LINES), HIGHLIGHTING THE CRZ. CENTRE COLUMN: TIME-AVERAGED MIXTURE FRACTION FIELDS WITH PSEUDO-STREAM LINES AND FI. RIGHT COLUMN: DISTRIBUTION OF INSTANTANEOUS FI VERSUS MIXTURE FRACTION. THE RIGHT AXIS SHOWS THE CUMULATIVE SUM OVER MIXTURE FRACTION OF TOTAL HEAT RELEASE RATE (GRAY), PREMIXED (CYAN) AND NON-PREMIXED (RED). VERTICAL LINES CORRESPONDS TO GLOBAL (YELLOW) AND STOICHIOMETRIC (GREEN) MIXTURE FRACTIONS.

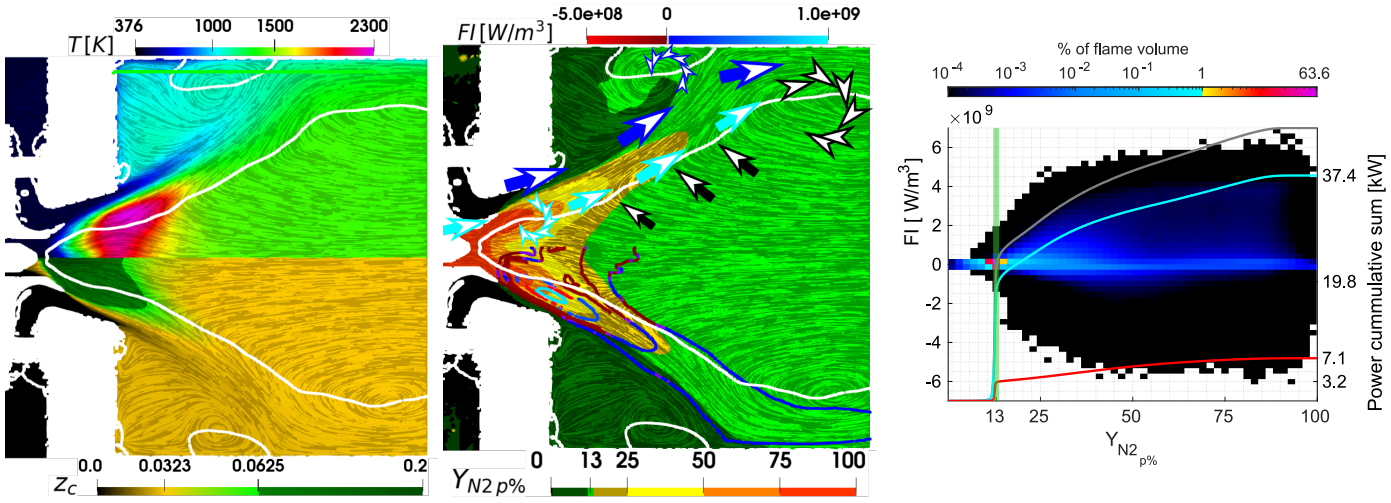

(a) OP_1

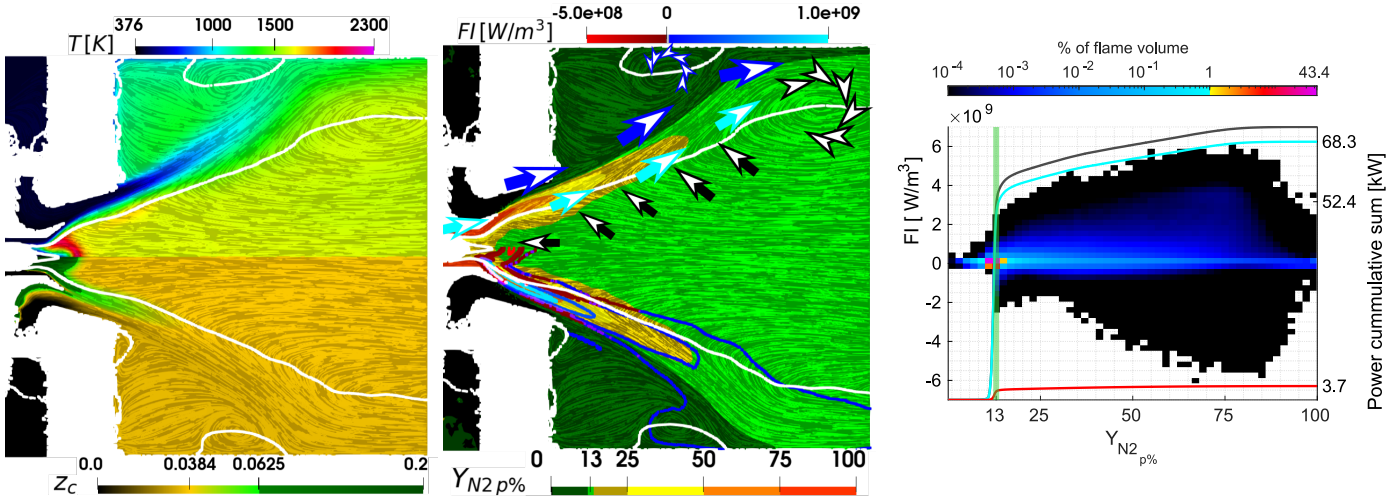

(b) OP_2

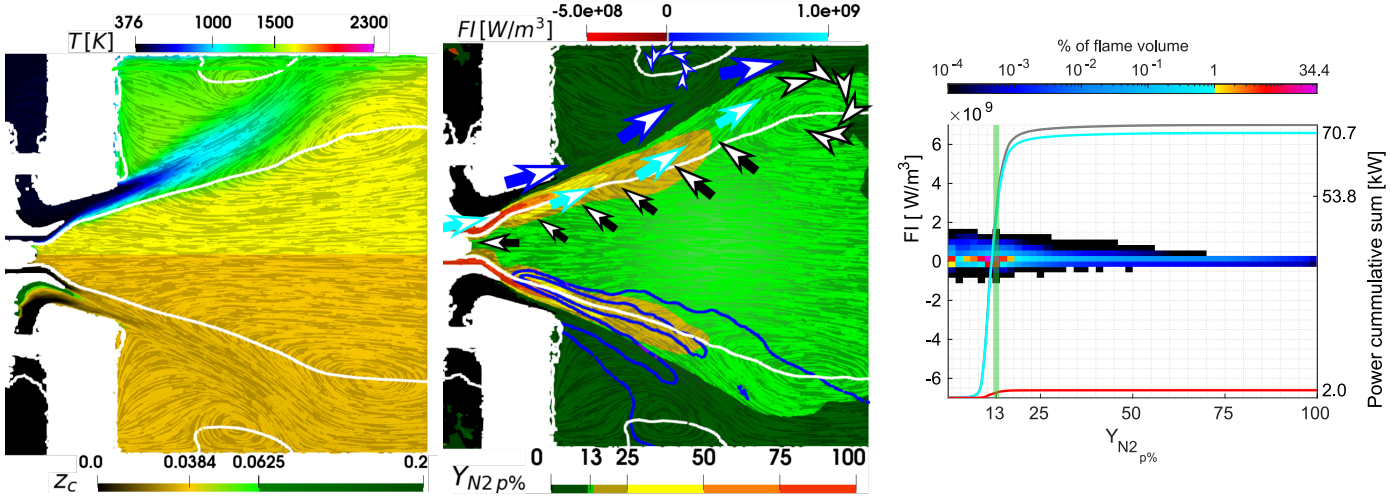

(c) $OP_{2,\alpha=0\%}$

FIGURE 3: V FLAMES. LEFT COLUMN: TIME-AVERAGED MIXTURE FRACTION WITH PSEUDO-STREAM LINES AND TEMPERATURE. CENTRE COLUMN: PILOT AIR PERCENTAGE ($Y_{N2\,p\%}$) FIELD. ON THE TOP, ARROWS INDICATE THE PATH OF MULTIPOINT (DEEP BLUE), PILOT (LIGHT BLUE) AND RECIRCULATING (BLACK) AIR. RIGHT COLUMN: DISTRIBUTION OF INSTANTANEOUS FI VERSUS PILOT AIR PERCENTAGE ($Y_{N2\,p\%}$). THE RIGHT AXIS SHOWS THE CUMULATIVE SUM OVER ($Y_{N2\,p\%}$) OF TOTAL HEAT RELEASE RATE (GRAY), PREMIXED (CYAN) AND NON-PREMIXED (RED) COMBUSTION. VERTICAL GREEN LINE CORRESPONDS TO THE GLOBAL AIR SPLITTING $Y_{N2\,p\%}$ = 13%.

responsible for the non-premixed combustion of the flame trunk than the reduced amount of air coming from the pilot stage.

The distribution of FI against the pilot air percentage (Fig. 3a) helps in confirming these behaviours for the different parts of the flame. It separates the non-premixed regime of the flame trunk (3.2 kW) from the one from the flame roots (3.9 kW), as the former is fed mainly by air from the CRZ on the equilibrium proportion, and the latter by higher quantities of pilot air. Finally, the flame branches, which burn mainly in the premixed regime, are mostly fed by multipoint air. Crossing the regions of these flame branches in the two averaged fields with two distributions confirms this behaviour, as almost the same power is produced by premixed combustion below the global equivalence ratio (20.7 kW below $z_{global} = 0.0323$) and by premixed combustion up to the air equilibrium proportion between stages (19.8 kW below $Y_{N2,p\%} = 13\%$), highlighting the role of the multipoint stage in promoting premixed despite the high staging factor.

The disproportionate distribution of fuel and air going through the pilot stage results in stoichiometric and fuel-rich combustion, and thus in very high temperatures (Fig. 2a), potentially leading to high pollutant emissions. These effects are intensified by the PVC in trapping the pilot air and by the flame trunk consuming oxygen that recirculates, reducing the availability of oxygen for the flame roots. Therefore, it is possible that in the absence of a PVC (thus with the pilot air having a conic trajectory) and with a pilot spray having injection angles closer to a true hollow cone (resulting in the absence of a flame trunk), the combustion regime of this $\alpha = 100\%$ V flame could be improved.

4.1.2 OP2. For the OP_2 V flame, the equivalence ratio is increased to $\phi = 0.57$, and the staging factor is decreased from $\alpha = 100\%$ to 15%. The change in staging factor considerably reduces the pilot injection and makes the equivalence ratio of each stage closer to the global equivalence ratio ($\phi_{pilot} = 0.66$, $\phi_{multi} = 0.56$). Figure 2b shows that, despite the strong pilot fuel mass flow rate reduction, the V flame is still attached and multi-regime, with non-premixed and premixed combustion regions divided between flame root, trunk and branches. However, despite the increase in global equivalence ratio, the OP_2 V flame burns much more in a premixed regime than the OP_1 V flame and the hot temperatures region is much reduced. Reducing the pilot fuel mass flow rate leads the flame root (anchored on the spray) and the flame trunk (between the spray and the burnt gases) to shrink and move upstream as the pilot spray droplets (green droplets in Fig. 2b) and the fuel-rich region it creates are much reduced and contained inside the divergent. This makes almost all of the fuel injected through the pilot injector be consumed by the flame roots and trunk and reduces by half the power emitted by non-premixed combustion compared to the OP_1 case, even if the OP_2 has a higher global equivalence ratio. Only a small portion of the pilot spray composed mostly of big droplets reaches the flame branches and the chamber walls, as shown in Fig. 2b.

The flame branches are mostly fed by the multipoint injection. In this injection system, the fuel is injected in the swirler vanes' exit, upstream of the divergent. The droplets then have more time to evaporate and mix, becoming much smaller than the ones injected through the pilot nozzle, as shown in Fig. 2b. Also in Fig. 2b, one can see that due to the jet-in-cross flow injection, the multipoint droplets spread from the internal to the external wall, with most of them sliding on the internal wall of the swirler (thus producing the rich mixture in this region in Fig. 2b). The ones that do not evaporate are dragged by the flow from the edge of the flow separator reaching the flame still as droplets and causing local non-premixed burning at the flame branches on the ISL. Also, the increase of fuel and droplets on the divergent walls creates a branch of flame over the ORZ, which did not exist in the $\alpha = 100\%$ case. As in OP_2 most of the fuel is being injected through the multipoint injector, this produces globally a much leaner mixture in the multipoint flow when compared to the one at the pilot nozzle exit. Therefore, the flame branches burn almost completely in lean premixed conditions, with only a small part of non-premixed combustion around some of the droplets. This increased the proportion of the flame that burns in the lean, premixed and low heat release rate regime. This is confirmed by the FI against mixture fraction and pilot air distributions (Figs. 2b and 3b). These graphs show that the premixed combustion produced by the flame branches corresponds to almost all of the flame volume and also to most of the emitted power (77%). The further comparison of these two distributions (Figs. 2b-3b) shows that part of the flame branches is now also fed by pilot air, as 55.4 kW are produced by premixed heat release around the global equivalence ratio, but only 52.4 kW is emitted around the 13% value corresponding to the equilibrium ratio of air between stages. Indeed, without the PVC, the pilot jet goes outwards conically, penetrating more towards the combustion chamber. The absence of the PVC and the conic trajectory of the pilot air also improves the mixing with the pilot spray portion, which has a similar trajectory. Therefore the flame root, which is now in the swirling jet and over the ISL, mostly burns in a premixed regime. This is confirmed by the pilot air distribution (Fig. 3b), which shows that the non-premixed combustion is concentrated inside the CRZ and occurs mainly at the global air splitting, while the premixed combustion also occurs for higher proportions of pilot air - because of the flame roots, as aforementioned.

The flame trunk is the only portion of the flame that still burns in a non-premixed regime. Indeed, its burning conditions are not optimal because, in this region, the fuel must interact with burnt gases to find the oxygen to burn. As the oxygen level of the burnt gases is already low, and the flow is much less turbulent than the fresh gas stream, this contributes to its richer non-premixed regime. The persistence of the flame trunk in these conditions might be due to the broad injection spray angle, still bringing fuel to the centre of the CRZ, and low turbulence inside the CRZ, characteristic of the CVB. However, the permanence of this small portion of non-premixed burning and elevated temperatures is desired, as it is expected to improve the flame's lean blow-off and stability limits ([32]). Nevertheless, in these conditions, the V flame produces 95% of its power in premixed conditions, which corresponds to the expected performance of an LPP system.

4.1.3 $OP_{2,\alpha=0\%}$. The last V flame is obtained after decreasing the staging factor to $\alpha = 0\%$. Associated withthe lack of fuel injection through the pilot stage, it leads to the extinction of the flame root and trunk, leaving a lifted flame composed of flame branches only(Fig. 2c). The combustion is almost completely done in a premixed regime at the global mixture fraction, while

only a marginal 3% of total power is produced in non-premixed conditions, a consequence of the accumulation of droplets near the walls and some isolated droplet burning. This is shown by the distribution of FI (Fig. 2c). Some of the combustion is done in slightly higher mixture fractions because the full multipoint injection concentrates fuel at the divergent's wall, thus increasing the equivalence ratio of the OSL branches of the flame. As this portion of the flame burns solely with multipoint air, this effect can be also explained by the multipoint stage equivalence ratio $\phi_{multi} = 0.65$ being slightly higher than the global equivalence ratio. Nevertheless, as the pilot air distribution shows in Fig. 3c, this flame benefits the most of both stages air, the OSL branches breathing the abundant multipoint air, while the ISL portions being fed with air at the equilibrium proportions or with a slightly higher proportion of pilot air (but not more than 25%). Thus, in this case, oxygen is not scarce in any flame region. Added with the lean and well-mixed mixture achieved by the multipoint injection system and the promoted fully premixed combustion, this leads to an average homogeneous low-temperature field (Fig. 2c).

In conclusion, these results show that the V flame shape responds ideally to fuel staging, going from a mostly non-premixed spray flame in pilot-only injection, to a fully premixed lean flame in multipoint-only conditions. The V flame shape creates two combustion zones, each preferentially fed by fuel and air coming from the two stages, which allows the flame to interact differently with them and to adapt to the desired features of each injector.

4.1.4 Precessing Vortex Core. For the V flames, a PVC was only present in the OP_1 case, where a pilot-only injection was used. This happens because the strong pilot spray creates the fuel-rich zone discussed in the previous section and shown in Fig. 2a. This strong spray and rich zone pushes the flame downstream, allowing the PVC to develop. As the staging factor is reduced, also reducing the fuel flow rate injected through the pilot nozzle, the flame moves upstream.Th suppresses the PVC, moving the CRZ upstream, thus engulfing the pilot nozzle and forcing the incoming gases outward, thus preventing the PVC from developing again even in the absence of a pilot flame.

Thus, in the OP_1 case, the PVC is very strong and the root of the flame follows its precessing movement, as it is placed just after the position of the PVC. Also, in these conditions, the PVC has an important role in improving mixing and helping spread the spray. The frequency of this PVC is around 1900 Hz in the simulation. It must be noticed that the signal of the PVC near the injector is so strong that it overshadows the acoustic quarter wave longitudinal mode ($f \approx 290$ Hz), which is barely present at this position. However, the effect of the PVC over the flame is only local, causing no excitation of the whole flame. Indeed, when a PSD is made over the whole heat release rate of the flame, only the acoustic quarter-wave mode of the flame is visible. For the OP_2 cases the flame moves upstream following the spray, and the PVC is suppressed. Even when the pilot flame is extinguished after the staging factor is further reduced to zero at the $OP_{2,\alpha=0\%}$ condition the PVC does not reappear, with both cases having very similar velocity and pressure fields close to the pilot injector. Thus, it is possible that the CRZ reaching far upstream up to the pilot nozzle pushes the flow outwards, preventing the PVC from appearing.

Nevertheless, there are strong interactions between the OP_2 flames and the ISL vortices, making it relevant to identify them as a Helical Vortex Core (HVC), as discussed by [33, 34]. The helical vortical structures wrinkle the flame, which is almost completely premixed in these regions (Fig. 2b), causing heat release rate oscillations. Nonetheless, this is different from what the PVC would do (as described in [35]), because the frequency of the ISL vortices varies according to their position over the ISL. As they interact with the acoustic mode by locking in the acoustic frequency [2], the interaction of the ISL and the flame acts as an intensifier of the acoustic mode, rather than exciting the flame in a higher characteristic frequency as the PVC. This is the reason why in this case only the acoustic mode is visible on the integrated heat release rate signal (see [36] for more details).

TABLE 2: OPERATING POINTS FOR THE TULIP FLAME

Point name	OP_1	OP_2
$\dot{m}_{air}$	$32.3 g/s$	$43.1 g/s$
T_{air}	$473K$	$433K$
$\dot{m}_{fuel}$	$1.02 g/s$	$1.64 g/s$
$Power$	$45.9 kW$	$73.9 kW$
α	100%	15%
ϕ, ϕ_{pilot}, ϕ_{multi}	0.47, 3.64, -	0.57, 0.66, 0.56

4.2 Tulip flames

The Tulip shape is a second type of attached flame that differs from the V flame. In [31], the tulip flame is meta-stable, obtained when the M flame flashbacks at around $\alpha = 20\%$. However, numerically, different paths for stabilising a Tulip flame were found. As shown in [16], a Tulip flame can be stabilised for OP_1. A second stable Tulip flame is obtained by changing the operating conditions from the OP_1 to OP_2 with $\alpha = 15\%$. The value of $\alpha = 15\%$ was chosen over the experimental $\alpha = 20\%$ because the Tulip flame was unstable at the latter. Furthermore, the Tulip at $\alpha = 15\%$ eases the comparison with the other two flame shapes also studied with OP_2 $\alpha = 15\%$ conditions. Therefore, a pilot-only and an LPP-like Tulip flame are studied and compared in this study, and the operating conditions are recalled in Tab. 2.

4.2.1 OP_1. The Tulip flame earns its name from the inwards closing of the flame branches, similar to a tulip flower (Fig. 4a). Thus, this shape is different from the V flames that shows a progressive and conic opening, because of its stabilisation over a Bubble Vortex Breakdown (BVB) mode, instead of the Conic Vortex Breakdown (CVB) of the V flame. Unlike the V flame, where both spray and ISL have a conic radial opening, the flame branches of the Tulip flame do not follow the spray (that still keeps mostly a conic radial opening) outwards, being rather stabilised by the closing ISL. The BVB flow topology increases the radial spreading of the fuel droplets, a consequence of the typical radial attraction by the CRZ that is in depression with respect to the swirling flow in a BVB mode. The CRZ depression is also responsible for the inward closing of the Tulip flame branches: as it attracts the droplets and fuel, the tulip flame branches follow the ISL, bending inwards. Also, this higher radial spreading and the increase in the ORZ, typical of the BVB topology, stabilise the flame over the OSL, which was not observed for the

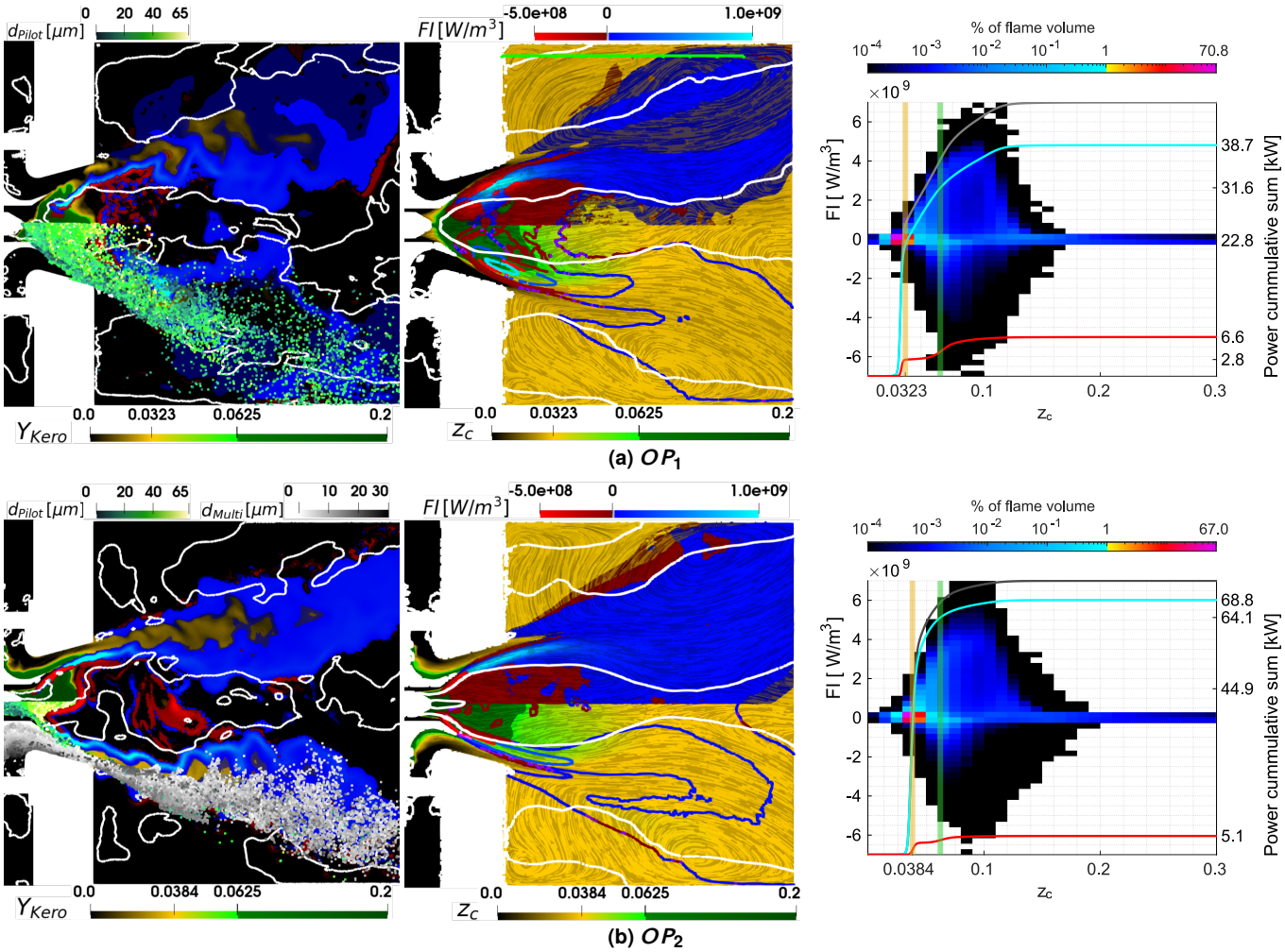

FIGURE 4: TULIP FLAMES. LEFT COLUMN: Y_{KERO} INSTANTANEOUS FIELDS WITH FI SUPERIMPOSED AND ISO-CONTOURS OF ZERO AXIAL VELOCITY (WHITE LINES), HIGHLIGHTING THE CRZ. CENTRE COLUMN: TIME-AVERAGED MIXTURE FRACTION FIELDS WITH PSEUDO-STREAM LINES AND FI. RIGHT COLUMN: DISTRIBUTION OF INSTANTANEOUS FI VERSUS MIXTURE FRACTION. THE RIGHT AXIS SHOWS THE CUMULATIVE SUM OVER MIXTURE FRACTION OF TOTAL HEAT RELEASE RATE (GRAY), PREMIXED (CYAN) AND NON-PREMIXED (RED). VERTICAL LINES CORRESPONDS TO GLOBAL (YELLOW) AND STOICHIOMETRIC (GREEN) MIXTURE FRACTIONS.

OP_1 V flame. Analysing the flame structure, Fig. 4a shows how the Tulip flame is stabilised in the chamber and highlights the burning regime. The roots of the flame are anchored at the rich mixture produced by the spray inside the CRZ, burning mostly in a non-premixed regime, as is the flame trunk, similar to the V flame. Indeed, comparing the attached parts on the average heat release rate fields for the OP_1 Tulip flame (Fig. 4a) and for the OP_1 V flame (Fig. 2a) one can see how very similar the flames are in this region despite the different flame shapes. Moreover, the aerodynamically stabilised parts of these flames also have a very similar structure, again despite the different shapes. The strong similarity of these flames is portrayed by the distribution of FI (Fig. 4a), showing almost identical results. Both cases present premixed and non-premixed combustion regimes mostly at the global mixture fraction (z_{global} = 0.0323) and in similar proportions: for the Tulip flame, 85% of the power is produced in premixed conditions, while 84% are for the V flame. In the premixed regime, for the Tulip case, 50% of the power is produced up to the global mixture fraction, while 47% are for the V flame. In the non-premixed regime, the Tulip flame delivers 42% of its power around the global mixture fraction, while the V flame produces 41% of it. This quantification confirms how similar these two flames are in terms of global structure.

The time average field of the pilot flow fictive variable (Fig. 5a) gives further insight into how each flame part is fed by air. The pilot air concentrates mainly in the divergent as the PVC brings it inside the CRZ. This feature is similar to the OP_1 V flame. As for the V flames, the fresh pilot air first reacts when reaching the flame root, then moves through the ISL, still reacting with the inner portion of the flame before reaching the CRZ. However, due to the BVB topology, a considerable difference is present for the Tulip flame, which impacts the combustion regime and the composition of the mixture inside the CRZ. Because of the BVB topology, the CRZ bubble attracts the pilot air inside it (as illustrated by the arrows in Fig. 5a), filling the CRZ mostly with burnt gases coming from the flame root. This phenomenon intensifies the non-premixed combustion regime of the flame trunk. This effect is reinforced by the CRZ being strangulated in the BVB topology, thus it is much harder for multipoint air to go inside the bubble. It is only for the CRZ portion that is downstream of

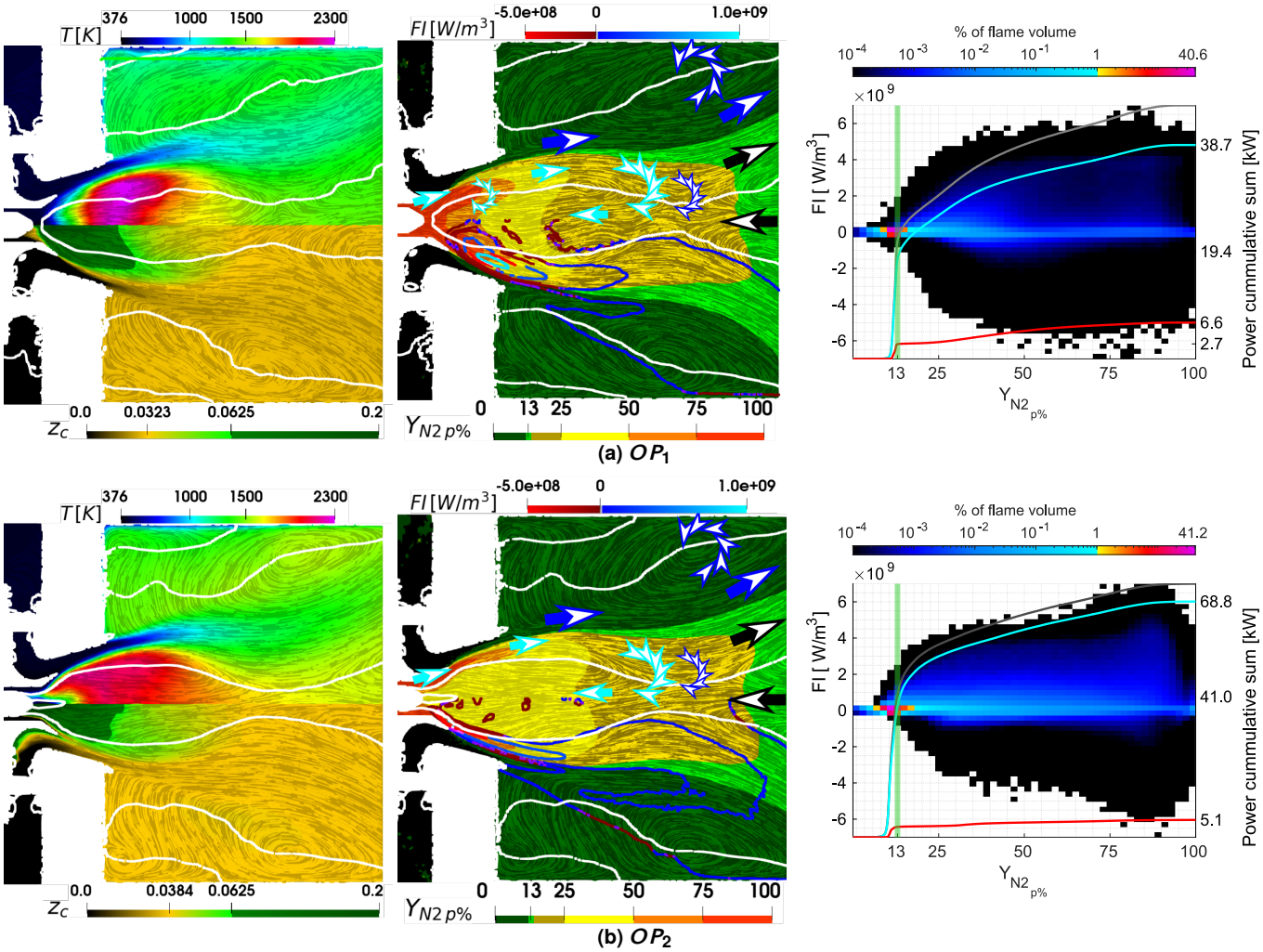

FIGURE 5: TULIP FLAMES. LEFT COLUMN: TIME-AVERAGED MIXTURE FRACTION WITH PSEUDO-STREAM LINES AND TEMPERATURE. CENTRE COLUMN: PILOT AIR PERCENTAGE ($Y_{N2\,p\%}$) FIELD. ON THE TOP, ARROWS INDICATE THE PATH OF MULTIPOINT (DEEP BLUE), PILOT (LIGHT BLUE) AND RECIRCULATING (BLACK) AIR. RIGHT COLUMN: DISTRIBUTION OF INSTANTANEOUS FI VERSUS PILOT AIR PERCENTAGE ($Y_{N2\,p\%}$). THE RIGHT AXIS SHOWS THE CUMULATIVE SUM OVER ($Y_{N2\,p\%}$) OF TOTAL HEAT RELEASE RATE (GRAY), PREMIXED (CYAN) AND NON-PREMIXED (RED) COMBUSTION. VERTICAL GREEN LINE CORRESPONDS TO THE GLOBAL AIR SPLITTING $Y_{N2\,p\%}$ = 13%.

the bottle-neck that the flow is in the air equilibrium proportion between stages of 13% of pilot air. This is very different from the V flame, which has the entire CRZ in the equilibrium proportion, thanks to its broader shape and higher recirculation flux. Finally, as for the V flame, the OSL portion of the flame branches is fed mainly by multipoint air for the Tulip flame.

The distributions of FI against the pilot air percentage identifies the impact of the flow topology on the flame interaction with each stage air. The OP_1 Tulip flame (Fig. 5a) shows an almost identical distribution compared to the corresponding V flame (Fig. 3a), as discussed in the previous section. Indeed, both present similar performances, as for the Tulip flame 50% of power delivered in the premixed regime and 41% of the power delivered in the non-premixed regime are produced with air below or at the equilibrium value of 13% of pilot air, while for the V flame, these values are 53% and 45%, respectively. The differences are precisely due to the distinct behaviours caused by the topology in the flame trunk combustion process.

4.2.2 OP_2. The strong reduction in pilot flow and pilot equivalence ratio (ϕ_{pilot} from 3.64 to 0.66) and the addition of the multipoint injection modify the local features of the tulip flame shape (Fig. 4b). The roots and trunk of the flame move upstream, a consequence of the reduced pilot fuel mass flow rate. The flame branches are also modified. As the multipoint droplets are much smaller, they follow the flow much more, better feeding the closing ISL inner branches of the flame than the pilot spray, which shows mostly a conic trajectory. This leads to the intensification of the ISL flame branches and much fewer droplets reach the walls. The change in staging also intensifies the OSL branches of the flame due to the sliding of the multipoint droplets on the walls of the divergent, compensating for the previous feeding of this region by the conic trajectory of pilot droplets.

Despite these local changes in the flame shape, the global structure of the OP_2 Tulip flame is very similar to the OP_1 case, as is its shape, shown by the FI instantaneous and average fields and its distribution (Fig. 4b). Indeed, the OP_2 FI distribution plot is a small shift to the right of the OP_1 one (as the equivalence

ratio increased from OP_1 to OP_2). Both the attached part and the branches of the flame are very similar for the two Tulips, with just the OSL part of the OP_2 Tulip flame burning more in a non-premixed regime, a consequence of the increase of multipoint droplets sliding over the divergent. The overall burning regime for the OP_2 Tulip is closer to the LPP expected operation: 93% is in the premixed regime, with 65% of it below the global mixture fraction ($z_{global} = 0.0384$), leading to a better LPP regime compared to OP_1. These values are close to the OP_2 V flame (95% of premixed combustion, with 81% below the global mixture fraction). Still, the V flame performs better, as it produces more premixed combustion below the global equivalence ratio and only produces around half of the total non-premixed combustion obtained for the Tulip flame. Indeed, for the Tulip archetype, changing the staging factor from $\alpha = 100\%$ to $\alpha = 15\%$ resulted in a much smaller reduction of non-premixed combustion (from 6.6 kW to 5.1 kW), showing that a significant amount of non-premixed combustion is intrinsic to the Tulip flame.

The pilot air field for the OP_2 Tulip flame (Fig. 5b) shows that the flow goes around the CRZ, as no PVC is present. This increases the axial penetration of pilot flow, favouring mixing with the multipoint air. Indeed, comparing Figs. 5a and 5b, one can see that for the OP_2 case, the $[50\%, 100\%]$ region is located in the fresh gases near the multipoint stream. Despite this difference, pilot air feeds the flame root and most of the ISL portion of the flame branches for both cases. However, the BVB topology hinders the air mixing inside the CRZ, as shown by the persistence of high pilot air inside the CRZ ($[25\%, 50\%]$ region, marked by the bright yellow colouring) when compared to the V OP_2 flame, which shows the whole CRZ in the equilibrium proportion. This shows that the BVB topology increases the proportion of non-premixed combustion. Finally, the OSL portion of the flame branches is barely modified, as it is fed by multipoint air.

It is interesting to analyse the pilot air versus FI scatter plot. Even though most of the Tulip flame burns below the equilibrium value of 13% of pilot air, a considerable portion of the points are spread onto the higher pilot air region (Fig. 5b), which does not happen for the V flame (Fig. 3b). This explains the better performance of the V flame in the LPP regime in terms of better distributing the combustion process between the air that comes from each stage. In the OP_2 case, for the Tulip flame, 59% of the total premixed heat release and 50% of the total non-premixed heat release occur below or at the air equilibrium value between stages of 13% of pilot air, while for the V flame, these values are 77% and 90%, respectively. This shows that the Tulip flame in LPP conditions still consumes more pilot air than it should, despite the lean equivalence ratio in each stage. Indeed, a considerable part of the Tulip flame OP_2 pilot spray consumes air from the CRZ bubble to burn and, in the BVB topology, the CRZ bubble is composed more of pilot air than the CRZ in the CVB topology. This shows that the BVB topology relies more on the pilot air, which is much more limited in quantity, to burn. Additionally, the weaker recirculating flow inside the bubble and the pilot spray penetrating more into the CRZ increase the presence of non-premixed combustion. All these points highlight the fact that the CVB mode performs much better than the BVB one in LPP conditions. In the CVB case, the air from each stage is better distributed over the flame, feeding different regions and interacting with fuel near the correct proportion.

The temperature fields reveal another strong difference between the Tulip (Fig. 4b) and V (Fig. 2b) OP_2 flames. For the V flame, changing to LPP conditions (OP_2 $\alpha = 15\%$) made almost non-existent very high temperature burnt gases due to stoichiometric combustion. This is not the case for the Tulip flame, which in OP_2 still has the entire CRZ bubble at a very high temperature 2200 K, while most of the corresponding V flame has its CRZ at 1600 K. Looking only at this temperature difference, it is expected for the Tulip flame to show a much higher NOx production than the equivalent V flame at OP_2 (to be confirmed).

In conclusion, the Tulip flame is little impacted by the change in fuel staging, as it maintains its diffusion spray flame structure for both pilot-only and LPP operating conditions. The BVB topology annihilates the benefits of a staged injection, still producing locally very high temperatures and, much likely, high levels of NOx and soot in all cases. Therefore, unlike the V flame, the Tulip flame shape does not respond well to fuel staging.

4.2.3 Precessing Vortex Core. As for the V flame, a PVC is only present for OP_1. Again, when the pilot spray is strong enough, it creates a fuel-rich zone downstream of the pilot nozzle inside the divergent. This pushes the flame downstream, creating space for the PVC to develop. For OP_1, the root of the Tulip flame interacts with the PVC, similarly to the OP_1 V flame, but in both cases only causes a local excitation of the flame. The frequency of the PVC (1900 Hz) is also similar to all other reacting or non-reacting 32 g/s cases. This shows that for OP_1, the PVC is independent of the flame shape, as the flame is downstream of the PVC and, thus, the flame shape should not affect the PVC. For OP_2, the reduction of the staging factor makes the root of the flame move upstream, close to the pilot nozzle, thus suppressing the PVC, as for the V flame. Also similarly to the V flame, the helical structures interact with the flame through the ISL, which is dominated by helical vortices that wrinkles the flame branches causing local changes in the heat release rate. However, the smaller CRZ of the BVB mode reduces the intensity of these interactions, when compared to the CVB mode CRZ.

4.3 M Flames

The M flame shape is a lifted and fully aerodynamically stabilised flame. It has neither a flame root nor a flame trunk, being composed only of flame branches, as the OP_2 $\alpha = 0\%$ V flame. It earns its name from the shape that arises from its stabilisation mechanisms: it has its external branches stabilised by the OSL and internal branches over the ISL. However, instead of being attached to the spray, the ISL branches are fully aerodynamically stabilised, uniting at the chamber's centre to create a leading edge inside the CRZ. The leading edge is stabilised at the end of the CRZ bubble, where the fresh gases enter the bubble. This entry of cold gases inside the bubble partially controls the axial position of the leading edge, as, because of it, the CRZ is too cold for the flame to propagate upstream further. Therefore, this also defines three parts for the M flame: OSL and ISL branches, and the leading edge. In the experimental work of [31] this flame has been only observed after the transition of the V flame LPP conditions (OP_2). Numerically, this flame could also be obtained after

TABLE 3: STUDIED OPERATING POINTS FOR THE M FLAME

Point name	$OP_{1,\phi=0.7}$	OP_2
$\dot{m}_{air}$	$32.3g/s$	$43.1g/s$
T_{air}	$473K$	$433K$
$\dot{m}_{fuel}$	$1.50g/s$	$1.64g/s$
$Power$	$68.8kW$	$73.9kW$
α	100%	15%
ϕ, ϕ_{pilot}, ϕ_{multi}	0.70, 5.37, -	0.57, 0.66, 0.56

ignition in pilot-only conditions [16]. However, when the equivalence ratio is reduced below $\phi = 0.7$, the M flame branches over the OSL extinct and the shape changes[19]. Thus, we study here the $OP_{1,\phi=0.7}$ pilot-only M flame instead. As explained in the next paragraphs, we do not think that this increase in equivalence ratio impacts the comparison with the other two flame shapes at the OP_1 conditions, as the M flame is very little impacted by changes in operating conditions. The OP_2 LPP M flame, as found by [31], is also studied as the other shapes. The operating parameters for the M flames studied here are listed in Tab. 3.

4.3.1 $OP_{1,\phi=0.7}$. The $OP_{1,\phi=0.7}$ M flame is shown in Fig. 6a. Despite being entirely inside the combustion chamber, because of the pilot-only injection and equivalence ratio $\phi = 0.7$, the leading edge is close to the fuel-rich zone created by the pilot spray inside the CRZ bubble. The spray penetrates up to the complete length of the CRZ bubble, filling it with droplets and evaporated fuel. On the positive axial flow jet, the spray spreads radially much more than in the CVB case, due to the central attraction caused by the CRZ depression characteristic of the BVB. The spray interacts mainly with the branches of the flame stabilised over the OSL and contributes significantly to stabilising the flame part that crosses the fresh air jet between the ORZ and the CRZ. Almost no droplet interacts with the portion of the flame inside the CRZ, as to reach it the droplets must reach the wall and recirculate, most of them being completely evaporated by then. The OSL branches of the M flame suffer periodically from the influence of vortex shedding at the entry of the chamber, giving it a "C" shaped curls just after where the OSL branches are attached. As shown in Fig. 6a the $OP_{1,\phi=0.7}$ M flame burns mostly in the premixed regime, showing how well the premixing works for this flame, despite the pilot-only injection. As the M flame is at a greater distance from the spray when compared to the V and Tulip ones, the fuel can mix well with the incoming air, and almost all of the heat released comes from mixture fractions up to the global value. However, the pilot injection contributes to non-premixed combustion on the flame OSL branches due to combustion around the large droplets. This is confirmed by the distribution in Fig. 6a, showing that only 84% of the total power is produced in a premixed regime. Thus operating with an M flame seems risky, as there is no evident gain in operating it with a pilot-only injection. Indeed, this flame shape is much more prone to lean blow-off than the other two under pilot-only injection. The leanest an M flame can be stabilised at pilot-only injection is at $\phi = 0.7$, being blown-off at lower values [19]. This is probably because the pilot droplets are too big to allow a burning rate at the OSL that can compensate for the heat losses.

Figure 7a shows the time-averaged fields of the percentage of pilot air, highlighting how the $OP_{1,\phi=0.7}$ M flame is fed with air. The CRZ bubble concentrates the pilot air, thus we can conclude that this is a characteristic of the BVB mode, as this is also the case for the Tulip flame (Fig. 5a). Here, the pilot flow also presents two major entry regions inside the CRZ. First, it is forced inside the CRZ by the PVC. The portion that escapes the PVC and continues to flow downstream is then pushed inside the CRZ by the bubble's depression. In opposition, the multipoint flow goes into the chamber from the divergent and separates into two paths: the more external portion goes into the chamber and to the ORZ, while the internal portion enters the CRZ by the bubble attraction and by the interaction with the ISL vortices. Therefore, as the flame is well downstream inside the chamber, mainly behind the CRZ bubble, it interacts with air at the equilibrium value of 13% of pilot air. Furthermore, Fig. 7a shows that the pilot flow concentrates mainly in the CRZ bubble, thus before the flame, while in the burnt gases region, the air is in the equilibrium proportion, indicating that the air coming from each stage mixes before reacting. This is confirmed by the distribution in Fig. 7a, showing that almost all of the M flame is fed by air at the equilibrium ratio for both premixed and non-premixed combustion. The exception is the leading edge of the M flame, which can move axially depending on the chamber temperature [17], and can thus lie in the higher pilot air regions or more downstream depending on the temperature. For the $OP_{1,\phi=0.7}$ case the temperature is high enough so that the leading edge is inside the $[13, 50]$% pilot air range, as shown by Fig. 7a.

Like the other two flames, the M flame also presents a region of high oxygen consumption and high temperatures (Fig. 6a. This is a consequence of the combustion of the flame OSL branches, where droplets concentrate and non-premixed combustion occurs. Thus, this supports the argument that the M flame offers little advantage in pilot-only conditions considering its limitations and compared to the other flames. The temperature field (Fig. 6a) also gives essential insight into the stabilisation of the leading edge of the flame. As the fresh gases are attracted inwards by the bubble, part of them goes inside the CRZ before reaching the flame, thus filling the bubble. This creates a Cold Central Recirculation Zone (CCRZ), filled with fresh gases and rich in fuel (being mainly the CRZ bubble) and a Hot Central Recirculation Zone (HCRZ), a region downstream of the flame (as it places itself in the threshold between the CCRZ and the HCRZ). The axial position of the leading edge of the flame is controlled then by the HCRZ and the chamber's temperature [17]. The hotter the temperature in the HCRZ, the more upstream the leading edge of the M flame can be, as the mixing of hot burnt and cold fresh gases determines the existence of the leading edge at that position. Thus, in this premixed M flame, parameters such as the pre-heating temperature, global equivalence ratio and wall losses are important determining the location of the M flame leading edge inside the chamber (and potential flashback risks).

4.3.2 OP_2. From the $OP_{1,\phi=0.7}$ M flame, the operating condition is changed to OP_2 to study the M flame in the LPP regime. The OP_2 flame shows the characteristic M shape. It burns almost completely in a premixed regime (Fig. 6b), without any local high heat release rate and with combustion concentrated around

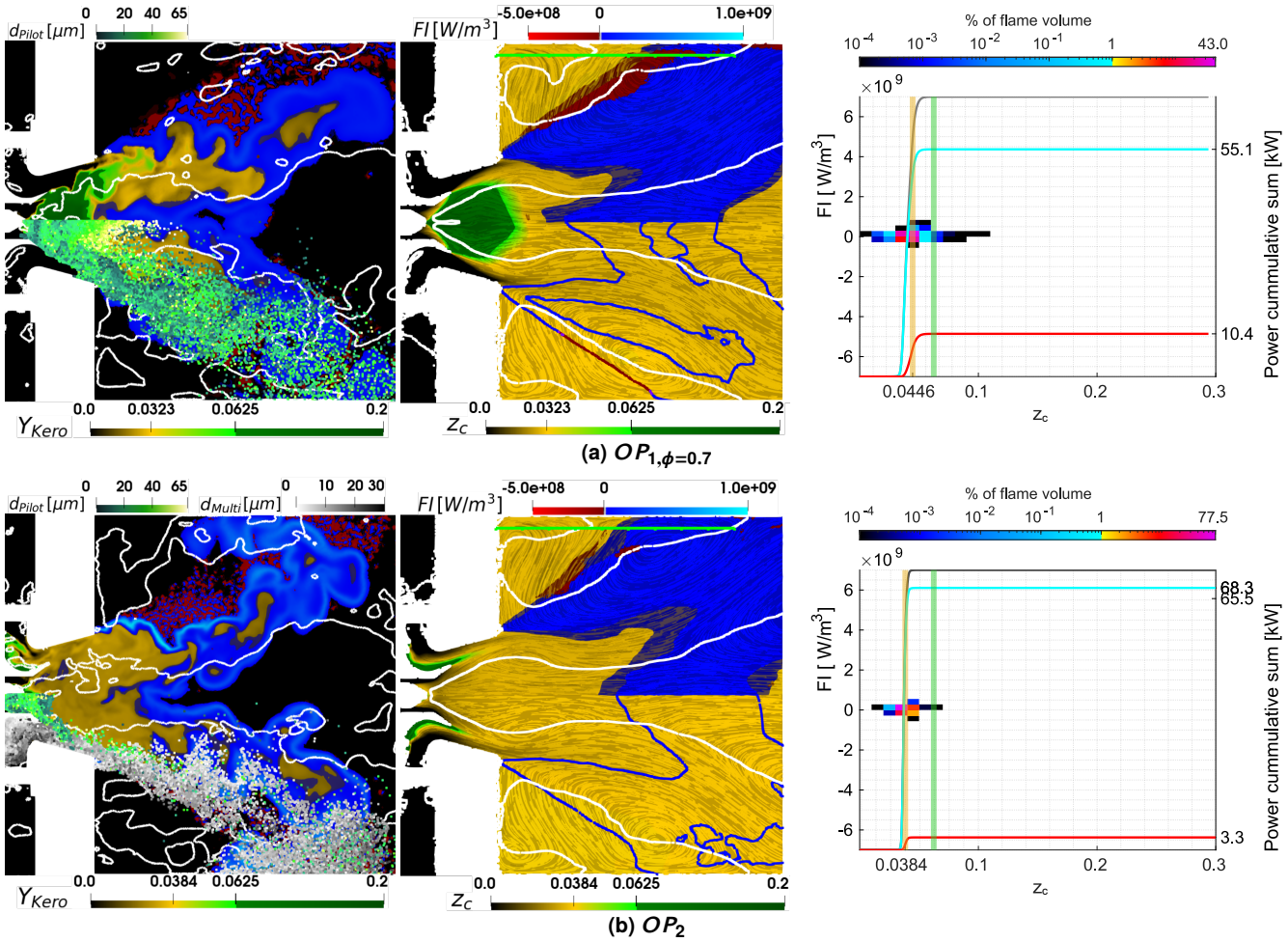

FIGURE 6: M FLAMES. LEFT COLUMN: Y_{KERO} INSTANTANEOUS FIELDS WITH FI SUPERIMPOSED AND ISO-CONTOURS OF ZERO AXIAL VELOCITY (WHITE LINES), HIGHLIGHTING THE CRZ. CENTRE COLUMN: TIME-AVERAGED MIXTURE FRACTION FIELDS WITH PSEUDO-STREAM LINES AND FI. RIGHT COLUMN: DISTRIBUTION OF INSTANTANEOUS FI VERSUS MIXTURE FRACTION. THE RIGHT AXIS SHOWS THE CUMULATIVE SUM OVER MIXTURE FRACTION OF TOTAL HEAT RELEASE RATE (GRAY), PREMIXED (CYAN) AND NON-PREMIXED (RED). VERTICAL LINES CORRESPONDS TO GLOBAL (YELLOW) AND STOICHIOMETRIC (GREEN) MIXTURE FRACTIONS.

the global lean mixture fraction. Compared to $OP_{1,\phi=0.7}$, the injection modification does not affect the shape or the stabilisation of the flame. However, the injection of smaller droplets by the multipoint allows stabilising the M flame with an equivalence ratio as low as $\phi = 0.6$, because these droplet evaporate faster and are mostly carried by the flow, differently from the ones injected through the pilot nozzle. Thus, the flow carries the multipoint droplets and fuel to the divergent walls, which enables the stabilisation of the branches of the M flame on the OSL with an equivalence ratio as low as of $\phi = 0.6$. Looking at the fuel mass fraction field, one of the main differences between this LPP M flame and the pilot-only $OP_{1,\phi=0.7}$ one comes from the change in the liquid fuel spatial distribution. As in the OP_2 case most of the fuel is injected by the multipoint stage, the fuel-rich region downstream of the pilot injector is much reduced on the OP_2 M flame (Fig. 6b), help to reduce risks of flashback.

The distribution of FI versus mixture fraction also shows that almost all of the combustion is premixed and below the global equivalence ratio (91%), with droplets still marginally burning in the non-premixed regime on the OSL. The small diameter of droplets from the multipoint injection is responsible for this considerable improvement of the combustion regime on the OSL branches. The performance of the OP_2 M flame is comparable to the $OP_{2,\alpha=0\%}$ V flame, even if the V flame has a slightly better performance: 97% of premixed combustion compared to 95% for the M OP_2 flame. Nevertheless, these results show that the M flame performs much better with the multipoint-dominated operation and that the remaining non-premixed burning of isolated droplets is probably linked with the size of the droplets coming from the multipoint injector and not from a specific flame shape.

Figure 7b presents the averaged field of pilot air for the OP_2 flame. It shows an interesting difference for the ORZ flow between OP_2 and $OP_{1,\phi=0.7}$: it is composed of higher multipoint air proportion. This is likely due to the increase in air mass flow rate required for the OP_2 conditions, which increases the segregation between each stage air flow. This increase in multipoint air in the ORZ could be an additional factor mitigating the non-premixed combustion in the OSL that is seen for the $OP_{1,\phi=0.7}$ case, even if the smaller droplets from the multipoint stage seem to be the significant factor for the change in combustion regime. Therefore, even if changing the staging factor does not alter the flow topology, it changes the spatial distribution of air coming from

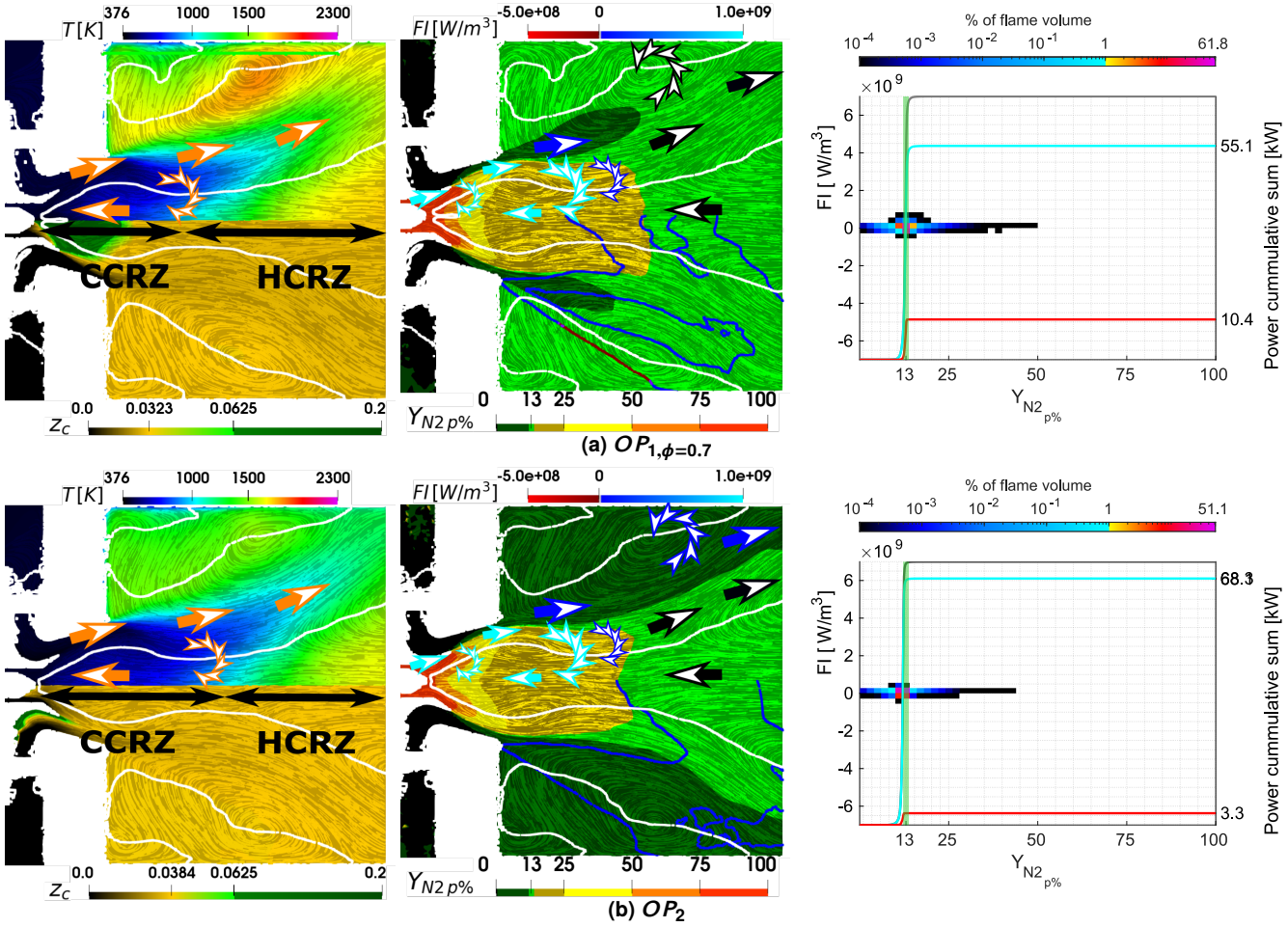

FIGURE 7: M FLAMES. LEFT COLUMN: TIME-AVERAGED MIXTURE FRACTION WITH PSEUDO-STREAM LINES AND TEMPERATURE. CENTRE COLUMN: PILOT AIR PERCENTAGE ($Y_{N2\,p\%}$) FIELD. ON THE TOP, ARROWS INDICATE THE PATH OF MULTIPOINT (DEEP BLUE), PILOT (LIGHT BLUE) AND RECIRCULATING (BLACK) AIR. RIGHT COLUMN: DISTRIBUTION OF INSTANTANEOUS FI VERSUS PILOT AIR PERCENTAGE ($Y_{N2\,p\%}$). THE RIGHT AXIS SHOWS THE CUMULATIVE SUM OVER ($Y_{N2\,p\%}$) OF TOTAL HEAT RELEASE RATE (GRAY), PREMIXED (CYAN) AND NON-PREMIXED (RED) COMBUSTION. VERTICAL GREEN LINE CORRESPONDS TO THE GLOBAL AIR SPLITTING $Y_{N2\,p\%}$ = 13%.

the stages, thus the high mass flow rate operation being more adapted to the M flame, as a considerable part of the burning is performed on the OSL branches. Finally, the scatter plot of Fig. 7b confirms that the M flame is stabilised in the regions with air in the equilibrium ratio, except for the leading edge, that goes into the higher regions of pilot air inside the CRZ bubble.

The time-averaged temperature (Fig. 6b) field shows again that the flame separates the CRZ into a cold region (CCRZ) and a hot region (HCRZ). Also, one can see that the burnt gases temperature is mostly low and uniform when compared to the attached flames, even in the regions where non-premixed burning is found. However, in this case the local highest temperatures of around 1800K are found in the CRZ. The average temperature field also highlights an important difference between the $OP_{1,\phi=0.7}$ (Fig. 6a) and OP_2 (Fig. 6b) M flames: the impact of the reduction of the equivalence ratio in the axial location of the leading edge of the flame. Reducing the equivalence ratio from $\phi = 0.7$ to $\phi = 0.6$ reduces the final combustion temperature in the CRZ. As the leading edge is in the intersection of the fresh gases that enter the bubble and the HCRZ, a colder HCRZ reduces the temperature inside the CRZ bubble, moving then the leading edge downstream when conditions are changed. This shows that the leading edge of the M flame is free to move axially and its axial position inside the CRZ can be changed based on global control parameters (mainly the equivalence ratio), the topology only imposing it to be around the centreline inside the CRZ [17].

In conclusion, these results show that the M flame shape and structure are very little impacted by the staging factor, burning in lean premixed conditions regardless of the injection strategy. Furthermore, not only fuel and air mix before reacting, but also the air coming from each stage mix between themselves and reach the equilibrium proportion before reacting. Thus, for the M flame there is little interest in having two different injection systems. The staging factor does not offer an efficient active control tool to adapt the combustion regime for the operation of an M flame. Moreover, increasing the staging factor increases the lean extinction limit of the burner when an M flame is stabilised (compared to V and T flames), and the risk of flashback, as shown by the fuel-rich zone in front of the OP_1 M flame leading edge and in the flashback study of [17]. In conclusion, the M flame is not adapted to varying staging factor systems, as it puts in risk stable operation, but rather a flame that is much more adapted to LPP pure operation only, sustained by a multipoint injection system.

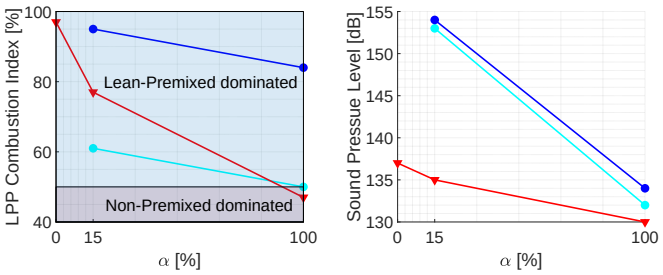

FIGURE 8: EVOLUTION IN FUNCTION OF STAGING FACTOR (α) OF: LPP COMBUSTION INDEX (LEFT) AND SPL RIGHT) FOR V (RED), TULIP (CYAN) AND M (BLUE) FLAMES. THE SYMBOLS REPRESENT DATA POINTS OF THE SIMULATIONS.

4.3.3 Precessing Vortex Core. A PVC is present for all M flames, as this flame shape is completely located inside the combustion chamber and the PVC can freely install itself and process around the pilot nozzle. The precessing frequency of the PVC once again increases with the increase in air flow rate, going from 1900 Hz for $OP_{ig,hp}$ (as in the other flames) to around 2200 Hz for OP_2. These frequencies are very close to the values observed for OP_1 and OP_2 non-reacting cases, respectively 1875 Hz and 2329 Hz, showing once again that the M flame keeps the same flow topology as the non-reacting flow.

5. SUMMARY

The comparison of the three archetypes is summarised in Fig. 8. We define the LPP Combustion Index as the percentage of total power produced by premixed combustion below global equivalence ratio. The Sound Pressure Level (SPL) is calculated using the pressure measurements at the half length of the chamber, at the same position where a microphone was placed during the experiments. Results shows that the V flame is the only one benefiting from the staging. The Tulip flame is not significantly altered by the change in staging. It keeps an important non-premixed combustion regime part for low staging, showing that the BVB mode nullifies the benefits of the staging strategy. On the other side of the burning regime spectrum, the M flame burns in a premixed-dominated regime for all staging values, offering no benefit of increased stability for higher staging values, as for the V flame. Finally, the M flame presents a bad performance for high pilot injection, producing local non-premixed combustion and high temperatures [17]. The M and Tulip flames are also more acoustically active than the V flame, offering a higher risk of combustion instabilities than the latter at all staging values, which reinforces the argument for considering a V flame. Therefore, this work argues that a V flame, and more generally speaking a CVB mode should be the target for staged burners to benefit from the fuel stratification strategy.

6. CONCLUSION

Three different flames observed in the BIMER combustor were investigated with LES to gain further insight into each flame archetype and to study the effect of fuel staging on them. In particular, we studied and compared for the first time the three flames in both high and low staging factor values. This allowed the evaluation of the impact of the staging factor on each flame archetype and thus their suitability for a staged burner operation.

After careful and detailed analysis, this work has demonstrated that a CVB mode V flame shape is the only one that responds optimally to fuel staging. The V flame can be changed from a mostly non-premixed spray flame to a completely premixed flame, depending on which injection system is used. Moreover, the V flame combustion regime responds proportionally when a combination of the two injectors is used. Therefore, we argue that similar flow and flame topologies and the presented methodology could be a first iteration for the flame shape and flow topology downselection for the design of lean-burn combustors.

ACKNOWLEDGMENTS

This work was granted access to the HPC resources of CINES under the allocation A0012B00164 made available by GENCI, and of the mesocentre computing centre of CentraleSupélec and Ecole Normale Supérieure Paris-Saclay supported by CNRS and Region Ile-de-France (http://mesocentre.centralesupelec.fr/). We finally thank CentraleSupélec and Université Paris-Saclay for Léo's Ph.D. grant, and CERFACS for sharing the AVBP solver.

REFERENCES

[1] Ducruix, S., Schuller, T., Durox, D. and Candel, S. "Combustion Dynamics and Instabilities: Elementary Coupling and Driving Mechanisms." *Journal of Propulsion and Power* Vol. 19 No. 5 (2003): pp. 722–734.

[2] Lieuwen, T. C. *Unsteady Combustor Physics*. Cambridge University Press.

[3] Billant, P., Chomaz, J. and Huerre, P. "Experimental study of vortex breakdown in swirling jets." *J. Fluid Mech.* Vol. 376 (1998): p. 183–219.

[4] Lucca-Negro, O. and O'Doherty, T. "Vortex breakdown: a review." *Prog. Energy Comb. Sci.* Vol. 27 (2001): pp. 431–481.

[5] Sarpkaya, T. "On stationary and travelling vortex breakdowns." *J. Fluid Mech.* Vol. 45 No. 3 (1971): pp. 545–559.

[6] Santhosh, R., Miglani, A. and Basu, S. "Transition in vortex breakdown modes in a coaxial isothermal unconfined swirling jet." *Phys. Fluids* Vol. 26 No. 4 (2014): p. 043601.

[7] Rajamanickam, K. and Basu, S. "Insights into the dynamics of conical breakdown modes in coaxial swirling flow field." *J. Fluid Mech.* Vol. 853 (2018): p. 72–110.

[8] Han, X., Laera, D., Morgans, A. S., Lin, Y. and Sung, C. "The Effect of Stratification Ratio on the Macrostructure of Stratified Swirl Flames: Experimental and Numerical Study." *J. Eng. Gas Turb. and Power* Vol. 140 No. 12 (2018): p. 121004.

[9] Han, X., Laera, D., Morgans, A. S., Sung, C. J., Hui, X. and Lin, Y. Z. "Flame macrostructures and thermoacoustic instabilities in stratified swirling flames." *Proc. Combust. Inst.* Vol. 37 No. 4 (2019): pp. 5377–5384.

[10] Taamallah, S., Dagan, Y., Chakroun, N., Shanbhogue, S. J., Vogiatzaki, K. and Ghoniem, A. F. "Helical vortex core dynamics and flame interaction in turbulent premixed swirl combustion: A combined experimental and large eddy simulation investigation." *Phys. Fluids* Vol. 31 No. 2 (2019): p. 025108, Publisher: American Institute of Physics.

[11] Chterev, I., Foley, C. W., Foti, D., Kostka, S., Caswell, A. W., Jiang, N., Lynch, A., Noble, D. R., Menon, S., Seitzman, J. M. and Lieuwen, T. C. "Flame and Flow Topologies in an Annular Swirling Flow." *Combustion Science and Technology* Vol. 186 No. 8 (2014): pp. 1041–1074.

[12] Malbois, P., Salaun, E., Frindt, F., Cabot, G., Renou, B., Grisch, F., Bouheraoua, L., Verdier, H. and Richard, S. "Experimental Investigation With Optical Diagnostics of a Lean-Premixed Aero-Engine Injection System Under Relevant Operating Conditions." 2017. American Society of Mechanical Engineers Digital Collection.

[13] Langella, I., Heinze, J., Behrendt, T., Voigt, L., Swaminathan, N. and Zedda, M. "Turbulent Flame Shape Switching at Conditions Relevant for Gas Turbines." *J. Eng. Gas Turb. and Power* Vol. 142 No. 011026 (2019).

[14] Soli, A. and Langella, I. "Numerical Investigation of a Coupled Blow-Off/Flashback Process in a High-Pressure Lean-Burn Combustor." *J. Eng. Gas Turb. and Power* (2022).

[15] Cheneau, B., Vié, A. and Ducruix, S. "Characterization of the hysteresis cycle in a two-stage liquid-fueled swirled burner through numerical simulation." *Proceedings of the Combusion Institute* Vol. 37 (2019): pp. 5245–5253.

[16] Mesquita, L. C. C., Vié, A. and Ducruix, S. "LES of the Ignition of a Two-Phase Staged Swirling Burner: Influence of Ignition Location and Operating Conditions on the Flame Shape." *Turbo Expo: Power for Land, Sea, and Air*, Vol. Volume 4A: Combustion, Fuels, and Emissions. 2020.

[17] Mesquita, L. C.C., Vié, A. and Ducruix, S. "Flashback-induced flame shape transition in a two-stage LPP aeronautical combustor." *Proc. Combust. Inst.* (2022).

[18] Cheneau, B., Vié, A. and Ducruix, S. "Numerical Study of Flame Shapes and Structures in a Two-Stage Two-Injection Aeronautical Burner With Variable Fuel Staging Using Eulerian Large Eddy Simulations." *J. Eng. Gas Turb. and Power* Vol. 141 (2019).

[19] Mesquita, L.C.C. "Simulation and analysis of the shape, performance and stability of flames in a two-stage lean-burn aeronautical combustor." Ph.D. Thesis, Université Paris-Saclay, CentraleSupélec, EM2C. 2021.

[20] Gicquel, L.Y.M., Staffelbach, G. and Poinsot, T. "Large Eddy Simulations of gaseous flames in gas turbine combustion chambers." *Prog. Energy Comb. Sci.* (2012).

[21] Nicoud, F. and Ducros, F. "Subgrid-scale stress modelling based on the square of the velocity gradient tensor." *Flow, Turb. and Combustion* Vol. 62 No. 3 (1999): pp. 183–200.

[22] Colin, O. and Rudgyard, M. "Development of High-Order Taylor-Galerkin Schemes for LES." *J. Comput. Phys.* Vol. 162 No. 2 (2000): pp. 338 – 371.

[23] Poinsot, T. and Lele, S. "Boundary conditions for direct simulations of compressible viscous flows." *J. Comput. Phys.* Vol. 101(1) (1992): pp. 104–129.

[24] Poinsot, P. and Veynante, D. *Theoretical and Numerical Combustion*. CERFACS, Third Edition.

[25] Charlette, F., Meneveau, C. and Veynante, D. "A power-law flame wrinkling model for LES of premixed turbulent combustion Part II: dynamic formulation." *Combust. Flame* Vol. 131 No. 1–2 (2002): pp. 181 – 197.

[26] Mesquita, L. C. C., Vié, A. and Ducruix, S. "Large Eddy Simulations of a two-phase staged swirling burner using an Euler-Lagrange approach: validation of the injection strategy. GT2018-76125." *Proceedings of the ASME Turbo Expo 2018*. 2018. Oslo, Norway.

[27] Franzelli, B., Riber, E., Sanjosé, M. and Poinsot, T. "A two-step chemical scheme for kerosene–air premixed flames." *Combust. Flame* Vol. 157 No. 7 (2010): pp. 1364 – 1373.

[28] Cheneau, B., Vié, A. and Ducruix, S. "Large Eddy Simulations of a Liquid Fuel Swirl Burner: Flame Characterization for Pilot and Multipoint Injection Strategies. GT2015-42821." *Proceedings of the ASME 2015: Turbine Technical Conference and Exposition*. 2015. Montréal, Canada.

[29] Paulhiac, D., Cuenot, B., Riber, E., Esclapez, L. and Richard, S. "Analysis of the spray flame structure in a lab-scale burner using Large Eddy Simulation and Discrete Particle Simulation." *Combust. Flame* Vol. 212 (2020): pp. 25 – 38.

[30] Abramzon, B. and Sirignano, W.A. "Droplet vaporization model for spray combustion calculations." *Int. J. Heat and Mass Transfer* Vol. 32 (1989): pp. 1605–1618.

[31] Renaud, A. "High-speed diagnostics for the study of flame stabilization and transient behaviour in a swirled burner with variable liquid-fuel distribution." Ph.D. Thesis, CentraleSupélec. 2015.

[32] Lefebvre, A.H. and Ballal, D.R. *Gas Turbine Combustion (3rd Edition)*. Taylor and Francis, Philadelphia, USA.

[33] Caux-Brisebois, V., Steinberg, A.M., Arndt, C. M. and Meier, W. "Thermo-acoustic velocity coupling in a swirl stabilized gas turbine model combustor." *Combust. Flame* Vol. 161 (2014): pp. 3166–3180.

[34] Steinberg, A. M., Boxx, I., Stöhr, M., Meier, W. and Carter, C. D. "Effects of Flow Structure Dynamics on Thermoacoustic Instabilities in Swirl-Stabilized Combustion." *AIAA Journal* Vol. 50 No. 4 (2012): pp. 952–967.

[35] Steinberg, A. M., Boxx, I., Stöhr, M., Carter, C. D. and Meier, W. "Flow-flame interactions causing acoustically coupled heat release fluctuations in a thermo-acoustically unstable gas turbine model combustor." *Combust. Flame* Vol. 157 (2010): pp. 2250–2266.

[36] Mesquita, L. C.C., Vié, A., Zimmer, L. and Ducruix, S. "Numerical analysis of flame shape bifurcation in a two-stage swirled liquid burner using Large Eddy Simulation." *Proc. Combust. Inst.* Vol. 38 No. 4 (2021): pp. 5971–5978.

APPENDIX A. COMPARISONS WITH EXPERIMENTAL DATA

A.1 V flames

The three V flames were studied experimentally, but data for only OP_1 and OP_2 $\alpha = 15\%$ flames were available for validation.

For the OP_1 V flame, Fig. 9(top) compares the heat release rate extracted from the LES with the spontaneous emission of CH obtained during the experiments ([31]). The simulations retrieve the experimental V flame, the LES flame presenting a similar opening and the same stronger reacting regions at the exit of the

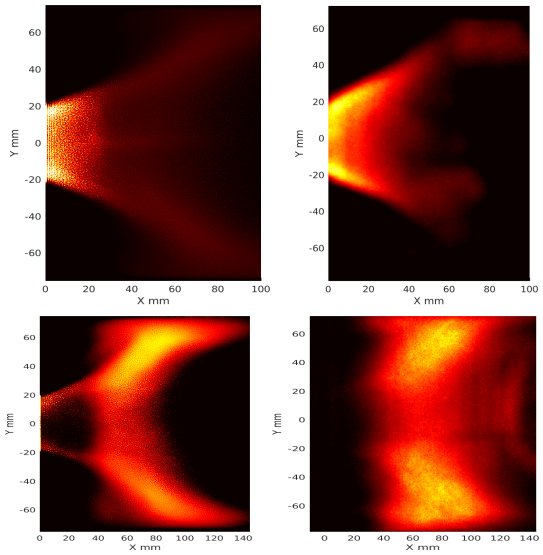

FIGURE 9: LES HEAT RELEASE RATE (LEFT) AND CH* CHEMILUMINESCENCE (RIGHT, [31]) FOR THE α = 100% (TOP) AND THE α = 15% (BOTTOM) V FLAME. ALL THE IMAGES ARE AVERAGED TEMPORALLY AND INTEGRATED ALONG THE LINE OF SIGHT.

divergent, as observed during experiments. Thus, since there is a strong resemblance in shape between chemiluminescence and LES, the OP_1 V CVB flame is believed to be correctly represented. For the OP_2 V flame, the comparison between the LES flame and the experimental one is presented in Fig. 9(bottom), with the same characteristics as for Fig. 9(top). The LES captures well the V flame and how different the V α = 15% flame is from the V α = 100% one. Now the strongest emission region is visible on the flame branches inside the chamber and near the wall, both showing a much longer and more spread flame. The LES captures well the intense signal at the end of the branches, and the signal spreading at the walls. Still, slight differences are visible. On the experimental side, the spontaneous emission signal is very low at the entrance of the chamber, whereas the simulation clearly shows the presence of heat release in this region.

A comparison between the droplets in experiments and in the LES is performed to assess the LES accuracy on the liquid phase. For the OP_1 V flame, Fig. 10 shows the SMD, axial and radial velocities. First, comparing the SMD average fields (Fig. 10a), one can see that the LES captures very well the radial spread of the droplets, when comparing the top half of the images, as the bottom part of the experimental measurements were compromised by the presence of the flame ([31]). The LES sends droplets to the centre of the CRZ, as in the experiments, showing that the calibration procedure done in [26] was important to retrieve a good spatial distribution of droplets in the reacting case. Analysing the axial velocity fields (Fig. 10b), an analogous result is retrieved, where the LES manages to send droplets to the centre of the CRZ. However, this field shows that, while in the experiments the droplets are more dispersed inside the CRZ, the LES concentrates droplets with an axial trajectory at the centre of the spray. This might imply that a higher variation of the internal angle of the spray would be needed for reacting conditions, but this hypothesis was not tested due to a limitation in computational

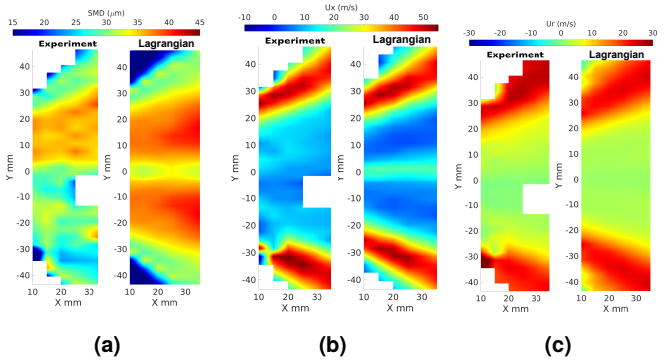

FIGURE 10: OP_1 α = 100% V FLAME: (A) SAUTER MEAN DIAMETER (SMD), (B) AXIAL AND (C) RADIAL MEAN VELOCITIES OF THE DROPLETS FOR THE EXPERIMENTS AND THE SIMULATION.

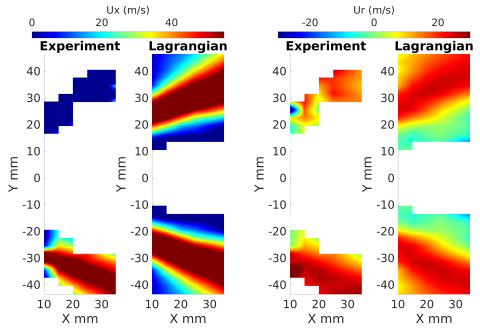

FIGURE 11: OP_2 α = 15% V FLAME: (A) AXIAL AND (B) RADIAL MEAN VELOCITIES OF THE DROPLETS FOR THE EXPERIMENTS AND THE SIMULATION.

resources. Nevertheless, the experiments show that the droplets inside the CRZ have positive axial velocity, as the LES and the magnitude of these velocities are similar. Additionally, the SMD field of the LES is very close to the top half of the experimental measurements, thus, these results give confidence that the modelling of the pilot spray is accurate for these simulations. Finally, the radial velocity fields (Fig. 10c), also portray the good agreement produced by the LES, especially inside the CRZ. Another important argument giving confidence to the LES and the calibration done in [26] is that it allowed a PVC to develop as in the experiments. This opposes the simulations with the original FIMUR, which placed the flame too close to the pilot injector, thus suppressing the PVC.

For the OP_2, Fig. 11 shows the comparison of velocity fields interpolated from the individual droplets' velocity components and attests that the LES captures well the behaviour of the droplets. Unfortunately, the presence of the flame prevents the accurate measurement of the SMD field and introduces some bias to the velocity fields. The upper side of the experimental results must be ignored, as the results are inaccurate. Very good agreement is still found when comparing the axial and radial velocity fields on the bottom halves, regions where sufficient experimental data were available. During the experiments of [31], the SPL were measured for the V flames for α = 100% and α = 15%: 131 dB (OP_1) and 135 dB (OP_2). These were measured with a microphone located at the top wall and at half of the chamber length. From the LES, the values measured at the same position

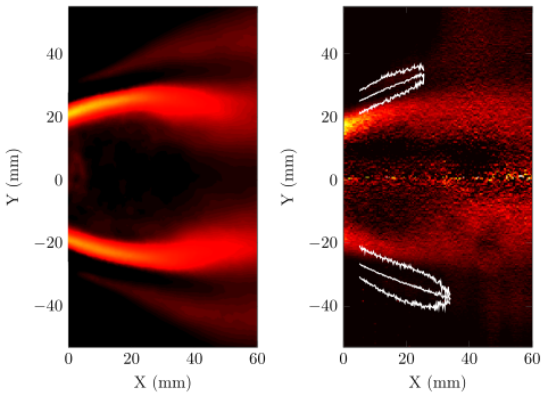

FIGURE 12: COMPARISON OF THE XY CUT OF THE AVERAGE HEAT RELEASE RATE FOR THE SIMULATION (LEFT) AND THE ABEL-INVERTED MEAN CH* CHEMILUMINESCENCE FROM THE EXPERIMENTS FOR THE TULIP FLAME. THE WHITE LINES REPRESENT THE SPRAY LIMITS FROM THE MIE SCATTERING RMS [31].

and conditions are 130 dB (OP_1) and 135 dB (OP_2), respectively. These results show that these LES can precisely reproduce the pressure oscillations found in the combustion chamber, mostly due to the acoustic longitudinal quarter-wave mode of the chamber.

A.2 Tulip flames

Only the OP_2 Tulip flame was observed experimentally for $\alpha = 20\%$, and the available data for validation resumes in $CH*$ chemiluminescence images, allowing flame-shape comparisons. Thus, the OP_2 $\alpha = 15\%$ LES Tulip flame shape is compared to the experiments abel-inverted mean $CH*$ chemiluminescence image of the $\alpha = 20\%$ Tulip flame in Fig. 12. The results show that the LES reproduce very well the Tulip shape, with the flame branches at the right position and with the inward closing very well captured. Also, the higher intensity of the ISL Tulip branches over the OSL branches is also well captured by the LES.

A.3 M flames

The only M flame studied during the experiments was the OP_2 one, thus it is compared here to the LES results. Figure 13 compares the heat release rate extracted from the LES with the spontaneous emission of CH obtained during the experiments ([31]). One can see that the LES captures well the M shape of the flame. A detail, however, that must be further investigated is the position of the leading edge. As the experimental image was slightly tilted to capture the flame at the exit of the divergent ([31]), one cannot be sure of the exact position of the leading edge observed experimentally. Nevertheless, it seems that the numerical flame has its leading edge slightly downstream than the experimental one. The OP_2 M flame is the only case with measurements for the spatial distribution of droplets. A comparison between the droplets measured during the experiments and the LES is presented in Fig. 14, showing the velocity fields interpolated from the individual droplets' velocity components. It is noted by [31] that, as for the V flame, the experimental measurements of the droplets were disturbed by the presence of the flame, impacting the quality of the measurements by undermining the presence of small droplets. This bias accounted for,

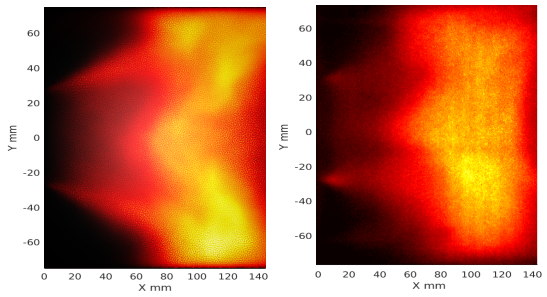

FIGURE 13: LES HEAT RELEASE RATE (LEFT) AND CH* CHEMILUMINESCENCE IMAGE (RIGHT, FROM [31]) FOR THE $\alpha = 15\%$ M FLAME. ALL THE IMAGES ARE AVERAGED TEMPORALLY AND INTEGRATED ALONG THE LINE OF SIGHT.

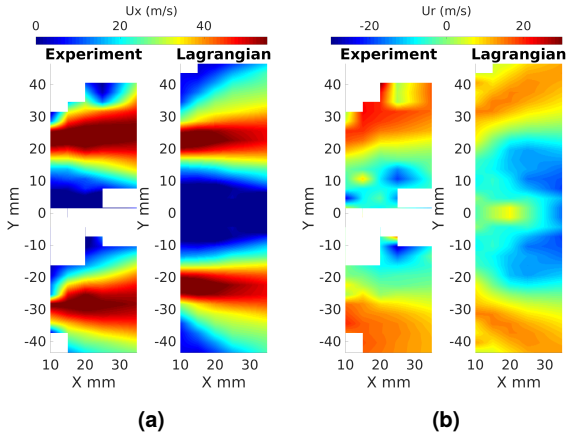

FIGURE 14: OP_2 $\alpha = 15\%$ M FLAME: (A) AXIAL AND (B) RADIAL MEAN VELOCITIES OF THE DROPLETS FOR THE EXPERIMENTS AND THE SIMULATION.

the results show that the LES captures well the behaviour of the droplets. The velocity fields present good agreement, showing the same tendencies and structures. It is important to mention how the droplets are captured by the change in direction caused by the CRZ bubble, showing a strong negative radial velocity where fresh gases are attracted inside the CRZ. This shows that not only gaseous fuel is attracted inside the bubble, but also small droplets.

The SPL was also measured by [31] for the OP_2 $\alpha = 15\%$ M flame, 145 dB, measured from a microphone located at the top wall and at the half of the chamber length. The LES overestimates this value, resulting in 154 dB (OP_2), contrary to the V flame. The $OP_{ig,hp}$ value from the LES M flame is also given for reference, 134 dB, showing that as for the other two flames, going from OP_1 to OP_2 increases the SPL in the chamber.

,